

1 **Response to Anonymous Referee #1**

2  
3 The manuscript shows an interesting study on the use of multiangular spectral measurements  
4 to describe the physiological status of the vegetation canopy in a complex  
5 tree-grass ecosystem. In this context it contributes to the research done within scientific  
6 networks such as Fluxnet, SpecNet , Eurospec, Optimise, etc. that have worked  
7 on the integration and standardization of in situ optical and flux-tower measurements  
8 with the ultimate goal of determining ecosystem fluxes in a spatially and temporally  
9 continuous mode. It is extremely difficult to obtain accurate/reliable in situ spectral  
10 measurements, particularly in a continuous and multiangular mode due to a number  
11 of potential errors caused by instrumental and environmental factors. Therefore, the  
12 manuscript represents a substantial contribution in that field due to the scientific significance of the in  
13 situ dataset analyzed. Also the study site selected in this paper is  
14 very interesting from the remote sensing perspective as, in this savanna ecosystems,  
15 the estimation of biophysical properties is still an issue owing to the challenge of determining  
16 some variables in a highly heterogeneous canopy. The research questions  
17 addressed are relevant and clearly fall within the scope of Biogeosciences.

18  
19 **Response: We would like to take the opportunity to thank the reviewer for these valuable comments. We**  
20 **found the review to be highly constructive and after implementing most of the revisions we feel the paper**  
21 **has improved a great deal.**

22  
23 Specific comments addressing particular scientific issues:

24  
25 1. Abstract and introduction are concise and summarize relevant research to provide  
26 context. However, in the introduction I miss a review of previous works on continuous  
27 multiangular hiperspectral observations for ecosystem monitoring such as the ones  
28 from T. Hilker using the AMSPEC system.

29  
30 **Response: A section reviewing previous works on continuous multiangular hyperspectral systems**  
31 **for monitoring ecosystems in situ is included in the revised introduction.**

32  
33 2. In the methods section some key information on data acquisition is missing. This  
34 information is necessary in order to properly interpret the results, especially in the case  
35 of the hyperspectral reflectance measurements but also for the ecosystem properties.  
36 In the manuscript there is only one paragraph describing hyperspectral reflectance  
37 data acquisition. Authors refer to the work of Huber et al (2014) for additional information,  
38 however, the importance of this data in the context of the paper justifies a  
39 more detailed description in the methods section. One of the key issues related with  
40 continuous spectral observations are the potential errors caused by instrumental and  
41 environmental factors. Those should be at least briefly described in the paper. Another  
42 important information which should be included regarding spectral measurements is  
43 the area observed by the sensor which, in this ecosystem, is assumed to be a mixture  
44 of trees, grass and tree-shadows at the different viewing angles (including nadir  
45 observations). This is a relevant issue because authors are building empirical models

46 comparing spectral measurements with some ecosystem parameters as GPP which  
47 results from the mixed contribution of the different ecosystem fractions and others (as  
48 is the case in biomass) where the information comes only from the grass fraction.

49  
50 **Response: Thanks, we have provided more information regarding the biomass sampling, the**  
51 **eddy covariance measurements, and the spectral radiometer measurements in the revised method**  
52 **section. Possible errors in the measurements are also mentioned in the revised manuscript.**

53 **Thank you very much for pointing out to us that it was unclear regarding the instantaneous**  
54 **field of view (IFOV) by the sensor; this requires a bit more elaborate explanation (also included**  
55 **in the revised manuscript). There is no influence from trees in the hyperspectral data set used in**  
56 **this manuscript as the entire IFOV constitutes of herbaceous ground vegetation. In the analysis**  
57 **for relationships between seasonal dynamics in ecosystem properties and hyperspectral**  
58 **reflectance, we used nadir observations. The site only constitutes of 3% tree cover, and there are**  
59 **neither trees nor shading of trees in the IFOV for the nadir observations. For the analysis of**  
60 **anisotropy, we used angular measurements measured between (12:00 and 14:00), and there is no**  
61 **influence of trees nor any tree shading for this part of the day in the IFOV of the angular**  
62 **measurements. It is emphasized in the revised manuscript that the IFOV covers only herbaceous**  
63 **vegetation.**

64 **The biomass measurements is also only covering the herbaceous vegetation. The FAPAR**  
65 **measurements are done in the vicinity of the tower containing the radiometers, and thereby**  
66 **influenced by the same herbaceous vegetation as the radiometric measurements. GPP and light**  
67 **use efficiency is based on eddy covariance data with a median 70% cumulative footprint of 388**  
68 **m. These estimates are thereby influenced by both herbaceous vegetation and the tree cover.**  
69 **However, as the tree cover is only 3%, we consider that the major part of these variables also**  
70 **depend on the herbaceous vegetation. Information regarding the fetch and footprint of the**  
71 **measured variables is included in the revised manuscript.**

72  
73 3. Another key issue in this paper is the representativeness of the empirical relations  
74 found. There is an obvious limitation of the dataset in the spatial domain as it is only one instrument  
75 providing spectral observations. However, for the temporal domain,  
76 there are a large number of observations (1.5 years) that would allow an independent  
77 validation by using only part of the observations to calibrate the statistical model and  
78 another one to validate it.

79  
80 **Response: In the parameterisation of the statistical models, we used a bootstrap simulation**  
81 **methodology where the datasets were copied 200 times (Richter et al., 2012). When bootstrapping,**  
82 **a data set with the same number of data points as included in the original data set is created;**  
83 **some of the data points are left-out, and some of the data points are included several times. We**  
84 **used the data points that were included within each bootstrap run to parameterise the models,**  
85 **whereas the remaining ones were used for validating the models. So for each of the 200 runs we**  
86 **parameterised a statistical model, which was validated against the left-out subsample by**  
87 **calculating a root-mean-square-error. We estimated a median and a standard deviation from the**  
88 **200 runs. This information is emphasized in the revised manuscript.**

89  
90 4. Authors should better justify the negative correlations found between NIR bands

91 and biomass. Previous works have demonstrated negative correlations in the visible  
92 but positive in the NIR both for total and green biomass (could the tree and shadow  
93 fractions of the ecosystem included in the sensor FOV be influencing this relationship?)  
94

95 **Response: Thank you very much for pointing this out to us, this is very interesting. As there are**  
96 **no trees in the IFOV of the sensors, the trees do not influence this relationship. The signal is**  
97 **based on reflectance from a IFOV only containing herbaceous vegetation. When fitting a**  
98 **correlation to vegetation water content, there is a positive correlation. But when the correlation is**  
99 **done versus dry weight biomass, these positive relationships to NIR HCRF turns negative. It is**  
100 **included in the revised discussion that these strong negative NIR HCRF correlation with dry**  
101 **weight biomass should be studied further to better understand the respective importance of**  
102 **canopy water and leaf internal cellular structure for the NIR HCRF of herbaceous vegetation**  
103 **characterised by erectophile leaf angle distribution (LAD).**  
104

105 5. An interesting issue addressed by the paper is the effects of sun and sensor viewing  
106 geometry on NDSI. Did the authors analyzed how the mixed effect of the different  
107 ecosystem fractions (proportions) observed by the sensor at the different observation  
108 angles is contributing to these directional effects? Discussion about the potential of  
109 this dataset for BRDF modeling would be needed.  
110

111 **Response: The mixed effect of different ecosystem fractions is a very interesting point, and it**  
112 **would make a very interesting future study. However, it would require that the entire system is**  
113 **put on a higher tower. At the present height of the tower, only herbaceous vegetation is seen.**

114 **It is included in the revised discussion that this data set can potentially also be used for BRDF**  
115 **(bidirectional reflectance distribution function) modelling.**  
116

117 Specific comments addressing formal/technical corrections: (Line/page numbers are  
118 referred to the marked up version of the manuscript)  
119

120 Abstract

121 Line 115. Use hemispherical conical reflectance factor (HCRF) instead of reflectance  
122 (also throughout the paper)  
123

124 **Response: Thank you for mentioning this. We have now included the terminology of HCRF**  
125 **throughout the manuscript and included a footnote in the introduction clarifying this.**  
126

127 Introduction

128 Lines 137-138. Review commas in these sentences  
129

130 **Response: This is taken care of.**  
131

132 Line 152-153. Suggest to change “: : indices are ratio type of indices” by “: :”those  
133 based on band ratios” in order to avoid repetition  
134

135 **Response: This is taken care of.**

136  
137 Line 175-176. Suggest to change “The influence from sun-sensor variations: : :” by  
138 “The influence of sun-sensor geometry: : :”

139  
140 **Response: This is taken care of.**

141  
142 Lines 177-179. Not only goniometers but also multiangular satellite data, as the one  
143 provided by Chris Proba, has been used to analyze these effects.

144  
145 **Response: We have now added the Chris-Proba, MISR and POLDER satellite instruments**  
146 **including refs.**

147  
148 Line 187. Avoid repetition in the same sentence “hyperspectral reflectance”

149  
150 **Response: This is taken care of**

151  
152 Materials and method  
153 Line 220. Review the sentence. : : :grass and (other) herbaceous vegetation: : :?

154  
155 **Response: This is taken care of.**

156  
157 Line 259. The second sensor head is a cosine receptor? If so, please specify

158  
159 **Response: This is taken care of.**

160  
161 Lines 311-312. How the ANIF thresholds for data filtering were established?

162  
163 **Response: The threshold values of 0.8 and 1.2 indicate that the bias due to directional effects in**  
164 **the NDSI related to the variable view zenith angles are not larger than 20%. This is the same**  
165 **threshold value as was chosen for the effects of variable solar zenith angles. This is included in**  
166 **the revised manuscript. Honestly, the chosen level of 20% is somewhat arbitrary; it is a**  
167 **compromise between not incorporating too large bias, and not excluding too much data.**

168  
169 Lines 313-317. Move to section 2.4

170  
171 **Response: This is taken care of.**

172  
173 Lines 369-370. Those relationships obtained using filtered or not filtered data? Please  
174 specify also for other ecosystem properties.

175  
176 **Response: They are based on filtered data, this is specified in the revised manuscript.**

177  
178 Figures

179  
180 Figure 1. I would suggest replacing pictures by a high resolution image with the location

181 of the towers and showing the area observed by the spectroradiometer. Additional  
182 information on the location of the biomass sampling plots and the EC mean footprint  
183 would be also useful.

184

185 **Response: This is a very good suggestion. We have decided to keep figure 1, but we included**  
186 **more photos in the figure. We have now photos of both towers, and the IFOV/footprint of both**  
187 **the spectroradiometers and the Eddy covariance measurements. In addition, we added a high**  
188 **resolution image includig the location of the towers, the biomass sampling plots and the EC**  
189 **footprint.**

190

191 Figure 5. How the authors explain the correlations peaks in all the graphs at approximately  
192 1200 nm? Also the information included in the figure caption would be quite  
193 useful in a separated table in the methods section summarizing the main characteristics  
194 of the different datasets (units, n) but also data range, aggregation (if any), data  
195 gaps, etc.

196

197 **Response: The correlation peak at about 1150 nm is caused by the water absorption peak around**  
198 **this wavelength (Thenkabail et al., 2012). The lower the reflectance in this peak, the higher the**  
199 **water content, and hence the higher the biomass. This information is included in the revised**  
200 **manuscript.**

201 **A table is included in the revised method section with the requested information.**

202

#### 203 **References:**

204 Richter, K., Atzberger, C., Hank, T. B., and Mauser, W.: Derivation of biophysical variables from  
205 Earth observation data: validation and statistical measures, APPRES, 6, 063557-063551-063557-  
206 063523, 10.1117/1.JRS.6.063557, 2012.

207

208 Thenkabail, P. S., Lyon, J. G., and Huete, A.: Advances in hyperspectral remote sensing of vegetation  
209 and agricultural croplands, in: Hyperspectral Remote Sensing of Vegetation, edited by: Thenkabail, P.  
210 S., Lyon, J. G., and Huete, A., CRC Press, Taylor and Francis Group, Boca Raton, FL, 3-35, 2012.

211

212

213 **Response to Anonymous Referee #2**

214  
215

216 The manuscript describes an interesting study using multi-angular hyperspectral data collected from a  
217 tower at a semi-arid savanna. Overall the study seems to have been undertaken in a scientifically  
218 appropriate manner and makes a valuable contribution to scientific progress. The scientific quality is  
219 high. And the presentation of the manuscript is of excellent quality.

220

221 While the data analysis is sound I have the following questions, comments and suggestions which  
222 should be addressed to improve the manuscript:

223

224 **Response: We would like to take the opportunity to thank the reviewer for valuable comments**  
225 **that we believe helped improving the revised version of the manuscript.**

226

227 The analysis of effects of varying sun / sensor geometry has been done over 15 days (of which 3 have  
228 been removed) during the peak of the growing season. This misses the highest zenith angles and times  
229 of different vegetation conditions. I suggest to repeat the analysis for other time periods as well to gain  
230 a full picture of sun / sensor geometry effects. Furthermore, why have only NDSIs been investigated  
231 and not the reflectances themselves? This information would help to understand the behaviour of the  
232 NDSIs and would support the claim in the discussion that NDSIs reduce angular effects.

233

234 **Response: The reason for not doing the analysis of the varying sun/sensor conditions at the point**  
235 **in time with the highest zenith angles, is that this occurs during the dry season (two months prior**  
236 **to the onset of the growing season) where there are no vegetation (herbaceous) influencing the**  
237 **reflectance spectrum in the measured area. The focus of the manuscript is to investigate how**  
238 **NDSI is coupled with vegetation parameters, and we hence choose to use the point in time with**  
239 **most vegetation on the ground.**

240

241 We agree that it would make a very interesting study to investigate how sun/sensor geometry  
242 influences NDSI differently across the year. However, this is not a minor task and this  
243 manuscript is long as is. We therefore feel that this is beyond the scope of this manuscript. But it  
244 is a very good idea for a future manuscript to investigate seasonal dynamics in anisotropy of both  
245 the reflectance spectrum on its own and on NDSI estimates. This is something that will hopefully  
246 be possible to do in a not too distant future.

246

247 The reason for focusing on NDSI, and not on the anisotropy on the reflectance values  
248 themselves is that it has already been done (Huber et al., 2014; Tagesson et al., 2015). The focus  
249 of the paper by Tagesson et al. (2015) is to present all research activities at the Dahra field site.  
250 Among them, a section of the anisotropy of the reflectance spectrum is presented. The aim of the  
251 paper by Huber et al. (2014) is to present the ASD set-up and investigate the quality of the  
252 measurements. A second aim is to study the effects of varying sun/sensor geometry on the  
253 reflectance spectrum. Therefore, in order not to present the same information two times, the  
254 effects of varying sun/sensor geometry part of this paper focus on the effects on the NDSI.

254

255 However, the comment is relevant and in the revised manuscript we have included a discussion  
256 regarding the behaviour of the NDSI in relation to the behaviour of the reflectance spectrum and  
257 referred to figures in Huber et al. (2014) and in Tagesson et al. (2015).

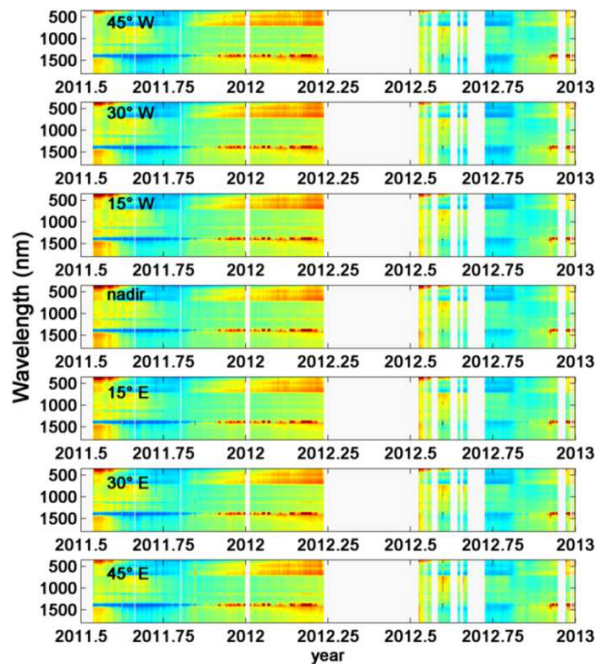
257

258 Why has the analysis of the relationship between reflectance / NDSI and ecosystem variables been  
259 restricted to a linear relationship? E.g. other studies found a non-linear relationship between reflectance  
260 and biomass due to saturation effects. Also why have only daily median reflectances / NDSIs been used  
261 when GPP, LUE and FAPAR were daily integrals? Averages would be more appropriate in these cases.  
262 And why have the off-nadir views not been analysed?  
263

264 **Response: In case the linear relationship is strong, it indicates limited issues with saturation. For**  
265 **wavelength regions where there are issues with saturations, exponential and logarithmic**  
266 **regressions could fit better. However, in case the aim is to find wavelength regions which are as**  
267 **sensitive as possible for investigating seasonal dynamics in an ecosystem property, wavelength**  
268 **regions with saturation issues should be avoided. Therefore linear models are better to use than**  
269 **non-linear models. This was the main reason for fitting linear rather than non-linear regressions.**  
270 **There is also a practical aspect to it, fitting the reduced major axis linear relationships using the**  
271 **bootstrapping methodology required a full month of processing for these 4 variables (GPP, LUE,**  
272 **FAPAR and biomass). In case we would try several other regression models, these would require**  
273 **several months of processing.**

274 **Median values were used in order to minimise the influence of errors in the analysis. Median**  
275 **provides the most common model output and it is thereby more robust against outliers than**  
276 **average values. This info was provided in the manuscript, but it was not mentioned the first time**  
277 **that median values were used. Thank you for pointing this out to us, it has been corrected in the**  
278 **revised manuscript.**

279 **We have investigated the seasonal dynamics in the off-nadir views as well, but as seen in the**  
280 **figure below, there was no difference in seasonal dynamics for the different viewing angles. We**  
281 **thereby choose to only use the nadir one, as it would not make any difference in the analysis.**



282  
 283  
 284  
 285  
 286  
 287  
 288  
 289  
 290  
 291  
 292  
 293  
 294  
 295  
 296  
 297  
 298  
 299  
 300  
 301  
 302  
 303  
 304

Some minor more specific comments:

page 3318, line 22: “Environmental conditions” usually mean variables like temperature, humidity, rainfall, etc. Do you mean reflectance in different wavelength regions have different sensitivity to “environmental conditions”? Or do you really mean “vegetation condition”?

**Response: Thank you for pointing this out. We meant variables like stand structure, health status of the vegetation, direct/diffuse radiation, vegetation and soil water content. This has been clarified in the revised manuscript.**

page 3320, section 2.1: It would be good to provide some information on the height of the grasses, trees and shrubs and the tree and shrub cover to get a better idea about the vegetation structure at the site.

**Response: In the revised manuscript information regarding the height of the trees and the herbaceous layer is included. Much more information regarding the footprint and the vegetation in the instantaneous field of view of the spectroradiometers are provided in the revised manuscript.**

page 3320, line 6: “(3%, of the land cover)”. remove comma.

**Response: This has been taken care of.**



305 page 3320, line 12: “rainfall (mm) was measured at 2m height”. Is the height relevant? Rainfall always  
306 has to be measured with the rain gauge not obstructed by any obstacles. What would be more  
307 interesting here is to know at what interval rainfall has been collected, i.e. daily, hourly, etc.  
308

309 **Response: All sensors were connected to a CR-1000 logger in combination with a multiplexer**  
310 **(Campbell Scientific Inc., North Logan, USA) and data were sampled every 30 s, and stored as 15**  
311 **minute averages (sum for rainfall). This info has been included in the revised manuscript.**  
312

313 page 3320, equation 1: Please define “albedo<sub>soil</sub>”. Has it been measured?  
314

315 **Response: Albedo<sub>soil</sub> is defined as PAR albedo of the soil, and it has been measured as 0.20**  
316 **(Tagesson et al., 2015). This info is included in the revised manuscript.**  
317

318 page 3321, line 19: Please define “VPD” on first use.  
319

320 **Response: This has been taken care of.**  
321

322 page 3322, section 2.4: The authors refer to Huber et al. (2014) for more detail on the spectrometer  
323 setup. However, the manuscript should provide some of the more fundamental information: 1. Were  
324 foreoptics used? 2. What are spectral resolution and spectral sampling of the spectrometers? 3. Have  
325 the seven different viewing angles been measured simultaneously? Or has a rotating or moving head  
326 been used? Was always the same target in the field of view? Or did the target change because of the  
327 rotating head? 4. How have solar irradiance measurements been made? Transmissive or reflective  
328 diffusor? 5. If multiplexing setup how long does it take to go through a whole measurement sequence?  
329 6. Has solar irradiance been measured for each view angle measurement separately?  
330

331 **Response: Thank you very much for pointing this out. Much more information about the**  
332 **spectroradiometer set-up is given in the revised manuscript, including information regarding all**  
333 **the points raised above.**  
334

335 page 3322, line 22: Why have daily median reflectances been used? Why not an average over a certain  
336 time interval?  
337

338 **Response: As mentioned above. We consider median values being more robust as they are not as**  
339 **sensitive to outliers and hence less affected by errors in the data set.**  
340

341 page 3323, line 6: “median” over what? The 15 days?  
342

343 **Response: Yes the median of the 15 days. This has been clarified in the revised manuscript.**  
344

345 page 3323, lines 19-22: I suggest to move the last sentence to the start of the paragraph, i.e. before line  
346 13 as the NDSI has to be calculated before the ANIF can be calculated.  
347

348 **Response: Thank you for this suggestion, it has been taken care of.**  
349

350 page 3325, line 5 + 22: Change “in the end” to “at the end”.

351

352 page 3329, line 15: Change “accurate and extra” to “additional”.

353

354 page 3329, line 25: Change “the majority” to “most”.

355

356 **Response: Thank you for these suggestions, they have been taken care of.**

357

358 page 3330, line 12: “Peak” suggests it is lower again at very high biomass. Rephrase.

359

360 **Response: We meant that the absorption of red light saturates at higher biomass loads. This has**  
361 **been changed in the revised manuscript.**

362

363 page 3330, lines 11-14: This is not the reason for the saturation of the NDVI. The NDVI saturates at  
364 high biomass because the NIR reflectance is much larger than the red reflectance. NDVI therefore  
365 reduces to  $R_{NIR} / R_{NIR}$  which equals 1.

366

367 **Response: We agree with you, and we are talking about the same thing, we are just using**  
368 **different phrasing, where you consider it from an equation point of view, we consider it from a**  
369 **leaf optical property point of view.**

370

371 **All vegetation indices using red will suffer from saturation problems. The reason for this is**  
372 **related to the fact that there are only so many photons striking a plant leaf and at a certain point,**  
373 **the chlorophyll absorbs nearly all the red energy to the point where no matter how much**  
374 **vegetation you add, more photons cannot be absorbed because they are already all absorbed. It is**  
375 **normally the red band that saturates. So any index using the red energy will suffer from the same**  
376 **limitation. For example, the Enhanced Vegetation Index (EVI) is not supposed to saturate as**  
377 **badly because in the equation empirical constants have been added to put more weight in the**  
378 **NIR spectrum that preserves sensitivity to higher loads of biomass (more layers of leaves) because**  
379 **here much more radiation is transmitted and reflected from the leaves.**

379

380 page 3330, lines 14-17: Again this is wrong. The saturation is not necessarily reduced with narrower  
381 bands. Narrow bands might even cause saturation earlier. Saturation can be reduced by selection of  
382 bands that show a smaller difference therefore avoiding the NDVI equation becoming 1 (see above).

383

384 **Response: Thank you for pointing this out for us. You are correct, it is not the narrowness of the**  
385 **band which results in that saturation is avoided, it is which wavelength region that is chosen.**  
386 **This has been clarified in the revised manuscript.**

387

388 page 3331, line 17-18: “As fluorescence is competing with photochemical conversion : : :” suggests  
389 high fluorescence equals low photochemical conversion. The reality is more complex. And it looks like  
390 often the opposite is true. So either remove this sentence or formulate differently.

391

392 **Response: Thank you again, this sentence is removed in the revised manuscript.**

393

394 page 3331, line 19-20: “: : should have very spectral high resolution (0.05-0.1nm)”. This is not true.  
395 Fluorescence has been measured successfully with a spectral resolution of about 10nm. Whether very  
396 high spectral resolution is necessary depends on the method applied.

397  
398 **Response: Thank for this comment; this also explains why we see such a strong peak even though**  
399 **the spectral resolution of the ASDs are 3 nm. This has been changed in the revised manuscript.**

400  
401 page 3332, lines 1-7: The whole discussion only focuses on what is happening at the leaf level, i.e.  
402 reduced pigment contents. What about changes in vegetation cover?

403  
404 **Response: Ok thanks. It has been clarified in the revised manuscript that the discussion is on the**  
405 **canopy level.**

406  
407 page 3342, Figure 2. Why are there gaps in the reflectance time series? Black vertical lines at the start  
408 and end of the rain seasons should be in all diagrams.

409  
410 **Response: The gaps are caused by technical issues due to loss of power supply, broken sensors or**  
411 **filtering of data due to bad weather conditions. This info is included in the revised manuscript.**  
412 **The black lines are included in all subplots in the revised manuscript.**

413  
414 **References**

415 Huber, S., Tagesson, T., and Fensholt, R.: An automated field spectrometer system for studying VIS,  
416 NIR and SWIR anisotropy for semi-arid savanna, *Remote Sens. Environ.*, 152, 547–556, 2014.  
417 Tagesson, T., Fensholt, R., Guiro, I., Rasmussen, M. O., Huber, S., Mbow, C., Garcia, M., Horion, S.,  
418 Sandholt, I., Rasmussen, B. H., Göttsche, F. M., Ridler, M.-E., Olén, N., Olsen, J. L., Ehammer, A.,  
419 Madsen, M., Olesen, F. S., and Ardö, J.: Ecosystem properties of semi-arid savanna grassland in West  
420 Africa and its relationship to environmental variability, *Global Change Biol.*, 21, 250-264, doi:  
421 10.1111/gcb.12734, 2015.

422  
423

424 **Relevant changes made in the manuscript**

- 425 • The word reflectance was changed to hemispherical conical reflectance factor.
- 426 • More information regarding the footprint/instantaneous field of view of the different sensor have  
427 been included.
- 428 • A table with sensor information has been included.
- 429 • More detailed information regarding the material and method has been included.
- 430 • A section reviewing previous works on continuous multiangular hyperspectral systems for  
431 monitoring ecosystems in situ is included in the revised introduction.
- 432 • A discussion regarding the behaviour of the NDSI in relation to the behaviour of the reflectance  
433 spectrum has been included.
- 434 • A discussion regarding the negative correlations between NIR HCRF and biomass has been  
435 included.
- 436
- 437

438

439 **Deriving seasonal dynamics in ecosystem properties of semi-**  
440 **arid savanna grasslands using from in situ based hyperspectral**  
441 **reflectance**

442  
443 **Torbern Tagesson<sup>\*1</sup>, Rasmus Fensholt<sup>1</sup>, Silvia Huber<sup>2</sup>, Stephanie Horion<sup>1</sup>, Idrissa Guiro<sup>3</sup>,**  
444 **Andrea Ehammer<sup>1</sup>, Jonas Ardö<sup>4</sup>**

445

446 <sup>1</sup>Department of Geosciences and Natural Resource Management, University of Copenhagen, Øster  
447 Voldgade 10, DK-1350 Copenhagen, Denmark; E-Mails: torbern.tagesson@ign.ku.dk, rf@ign.ku.dk,  
448 stephanie.horion@ign.ku.dk, andrea.ehammer@ign.ku.dk

449

450 <sup>2</sup>~~Danish Hydrological Institute~~, DHI GRAS A/S, Agern Allé 5, DK--2970 Hørsholm, Denmark; Ee-  
451 mail: shu@dhi-gras.com

452

453 <sup>3</sup>Laboratoire d'Enseignement et de Recherche en Géomatique, Ecole Supérieure Polytechnique,  
454 Université Cheikh Anta Diop de Dakar, BP 25275 Dakar-Fann, Senegal; Ee-mail: idyguiro@yahoo.fr

455

456 <sup>4</sup>Department of Physical Geography and Ecosystem Science, Lund University, Sölvegatan 12, SE--223  
457 62 Lund, Sweden, Ee-mail: jonas.ardo@nateko.lu.se

458

459 \*Correspondence to: Torbern Tagesson; torbern.tagesson@ign.ku.dk, Tel. nr: +46-704 99 39 36, Fax  
460 nr: +45 35 32 25 01, Department of Geosciences and Natural Resource Management, University of  
461 | Copenhagen, Øster Voldgade 10, DK-1350 Copenhagen, Denmark  
462

463 **Abstract**

464 This paper investigates how ~~seasonal~~ hyperspectral reflectance ~~data~~ (between 350 and 1800 nm) can be  
465 used to infer ecosystem properties for a semi-arid savanna ~~grassland ecosystem~~ in West Africa using a  
466 unique in situ based ~~multi-angular~~ dataset ~~of hemispherical conical reflectance factor (HCRF)~~  
467 ~~measurements~~. Relationships between seasonal dynamics in hyperspectral ~~reflectance~~HCRF, and  
468 ecosystem properties (biomass, gross primary productivity (GPP), light use efficiency (LUE), and  
469 fraction of photosynthetically active radiation absorbed by vegetation (FAPAR)) were analysed.  
470 ~~Reflectance~~HCRF data ( $\rho$ ) were used to study the relationship between normalised difference spectral  
471 indices (NDSI) and the measured ecosystem properties. Finally, also the effects of variable sun sensor  
472 viewing geometry on different NDSI wavelength combinations were analysed. The wavelengths with  
473 the strongest correlation to seasonal dynamics in ecosystem properties were shortwave infrared  
474 (biomass), the peak absorption band for chlorophyll a and b (at 682 nm) (GPP), the oxygen A-band at  
475 761 nm used for estimating chlorophyll fluorescence (GPP, and LUE), and blue wavelengths (FAPAR).  
476 The NDSI with the strongest correlation to: i) biomass combined red edge ~~reflectance~~HCRF ( $\rho_{705}$ ) with  
477 green ~~reflectance~~HCRF ( $\rho_{587}$ ), ii) GPP combined wavelengths at the peak of green reflection ( $\rho_{518}, \rho_{556}$ ),  
478 iii) the LUE combined red ( $\rho_{688}$ ) with blue ~~reflectance~~HCRF ( $\rho_{436}$ ), and iv) FAPAR combined blue  
479 ( $\rho_{399}$ ) and near infrared ( $\rho_{1295}$ ) wavelengths. NDSI combining near infrared and shortwave infrared  
480 were strongly affected by solar zenith angles and sensor viewing geometry, as were many combinations  
481 of visible wavelengths. This study provides analyses based upon novel multi-angular hyperspectral data  
482 for validation of ~~Earth-earth Observation-observation~~ based properties of semi-arid ecosystems, as well  
483 as insights for designing spectral characteristics of future sensors for ecosystem monitoring.

484 **1. Introduction**

485 Hyperspectral measurements of the Earth's surface provide relevant information for many ecological  
486 applications. An important tool for spatial extrapolation of ecosystem functions and properties is to  
487 study how spectral properties are related to in situ measured ecosystem properties. These relationships  
488 found the basis for up-scaling using earth observation (EO) data. Continuous in situ measurements of  
489 hyperspectral reflectance in combination with ecosystem properties are thereby essential for improving  
490 our understanding of the functioning of the observed ecosystems. Strong relationships have for  
491 example been found between information in the reflectance spectrum and ecosystem properties such as;  
492 leaf area index (LAI), fraction of photosynthetically active radiation (PAR) absorbed by the vegetation  
493 (FAPAR), light use efficiency (LUE), biomass, vegetation primary productivity, vegetation water  
494 content, and nitrogen and chlorophyll content , and vegetation water content (e.g. Thenkabail et al.,  
495 2012; Tagesson et al., 2009; Gower et al., 1999; Sjöström et al., 2009; Sims and Gamon, 2003). In situ  
496 observations of spectral reflectance are also important for parameterisation and validation of canopy  
497 reflectance models, and space and airborne products (Coburn and Peddle, 2006).

498 ~~Even though in situ measurements are fundamental for the EO research community, such datasets~~  
499 ~~are still rare and at the present state they do not cover different biomes at the global scale (Huber et al.,~~  
500 ~~2014).~~ There are vVery few sites across the world exist with an instrumental setup designed for multi-  
501 angular continuous hyperspectral measurements. ~~Even though continuous in situ measurements of~~  
502 multi angular hyperspectral HCRF are fundamental for the EO research community, such datasets still  
503 only cover a limited number of biomes at the global scale (Huber et al., 2014). Leuning et al. (2006)  
504 present a system mounted in a 70 m tower above an evergreen Eucalyptus forest in New South Wales



505 Australia, which measures spectral hemispherical conical reflectance factors (HCRF)<sup>1</sup> HCRF hourly  
506 throughout the year between 300 and 1150 nm at four azimuth angles. Hilker et al. (2007) and Hilker et  
507 al. (2010) describe an automated multiangular spectro-radiometer for estimation of canopy  
508 reflectance HCRF (AMSPEC) mounted on a tower above a coniferous forest in Canada. It sample  
509 s Spectral reflectance HCRF is sampled between 350 and 1200 nm year round under different viewing  
510 and sun angle conditions, achieved by and it is able to collection of data in a near 360° view around the  
511 tower with adjustable viewing zenith angles. E Even though in situ measurements of multi-angular  
512 hyperspectral HCRF are fundamental for the EO research community, such datasets are still rare and at  
513 the present state they do not cover different biomes at the global scale (Huber et al., 2014).

514 There are many methods for analysing relationships between hyperspectral reflectance and ecosystem  
515 properties, such as multivariate methods, derivative techniques, and radiative transfer modelling  
516 (Bowyer and Danson, 2004; Ceccato et al., 2002; Danson et al., 1992; Roberto et al., 2012). Still, due  
517 to its simplicity, the combination of reflectance into vegetation indices is the major method for up-  
518 scaling using EO data. By far, the most commonly applied vegetation indices are ~~the ratio type of~~  
519 ~~indices~~ those based on band ratios, e.g. the normalised difference vegetation index (NDVI), which is  
520 calculated by dividing the difference ~~in the reflectance HCRF~~ in the near infrared ( $\rho_{\text{NIR}}$ ) and red  
521 ( $\rho_{\text{red}}$ ) wavelength bands by the sum of  ~~$\rho_{\text{NIR}}$  the NIR~~ and  ~~$\rho_{\text{red}}$  red bands~~ (Tucker, 1979; Rouse et al.,  
522 1974). The ~~near infrared (NIR)~~ radiance is strongly scattered by the air-water interfaces between the  
523 cells whereas red radiance is absorbed by chlorophyll and its accessory pigments (Gates et al., 1965).  
524 The normalization with the sum in the denominator is a mean to reduce the effects of solar zenith

---

<sup>1</sup> Different reflectance terminologies have been used to inform on spectral measurements in the field by the remote sensing community leading to suggestions to the proper use of the terminology (Martonchik et al., 2000). All field spectro-radiometers measure HCRF (hemispherical conical reflectance) if the field of view (FOV) of the sensor is larger than 3° (Milton et al., 2009) and is therefore used throughout this paper to support the correct inference and usage of reflectance products (Schaepman-Strub et al., 2006; Milton et al., 2009).

525 angle, sensor viewing geometry, and atmospheric errors as well as enhancing the signal of the observed  
526 target (e.g. Qi et al., 1994; Inoue et al., 2008).

527 Wavelength specific spectral reflectance is known to be related to leaf characteristics such as  
528 chlorophyll concentration, dry matter content, internal structure parameters and equivalent water  
529 thickness (Ceccato et al., 2002). Hyperspectral reflectance data can be combined into a matrix of  
530 normalised difference spectral indices (NDSI), following the NDVI rationing approach. Correlating the  
531 NDSI with ecosystem properties provides a way for an improved empirically based understanding of  
532 the relationship between information in the reflectance spectrum with ground surface properties (e.g.  
533 Inoue et al., 2008). Several studies have analysed relationships between hyperspectral  
534 ~~reflectance~~HCRF, NDSI, and ecosystem properties (e.g. Thenkabail et al., 2000; Cho et al., 2007;  
535 Psomas et al., 2011; Inoue et al., 2008; Gamon et al., 1992; Feret et al., 2008; Thenkabail et al., 2012).  
536 Still, it is extremely important to examine these relationships for different ecosystems across the earth  
537 and investigate their applicability for different environmental conditions and under different effects of  
538 biotic and abiotic stresses.

539 A strong correlation between an NDSI and an ecosystem property does not necessarily indicate that  
540 the NDSI is a good indicator of vegetation conditions to be applied to EO systems. Visible, NIR and  
541 shortwave infrared (SWIR) have different sensitivity to variations in solar zenith angles, stand  
542 structure, ~~environmental conditions~~health status of the vegetation, vegetation and soil water content,  
543 direct/diffuse radiation ratio, and sensor viewing geometry. The influence ~~from of~~ sun-sensor ~~variations~~  
544 geometry on the reflected signal has been studied using radiative transfer models and airborne (e.g.  
545 AirMISR-) as well as satellite-based data from instruments; such as CHRIS-PROBA, MISR and  
546 POLDER (Huber et al., 2010; Maignan et al., 2004; Javier García-Haro et al., 2006; Jacquemoud et al.,  
547 2009; Verhoef and Bach, 2007; Laurent et al., 2011). However, effects of variable sun angles and

548 | sensor viewing geometries are not well documented [in situ](#) for different plant functional types of  
549 | natural ecosystems except for individual controlled experiments based on the use of field goniometers  
550 | (Sandmeier et al., 1998; Schopfer et al., 2008) ([e.g. Sandmeier et al., 1998](#)). Improved knowledge  
551 | regarding the influence from sun-sensor variability on different NDSI combinations is thereby essential  
552 | for validating the applicability of an NDSI for EO up-scaling purposes.

553 | The Dahra field site in Senegal, West Africa, was established in 2002 as an in situ research site to  
554 | improve our knowledge regarding properties of semi-arid savanna ecosystems and their responses to  
555 | climatic and environmental changes (Tagesson et al., 2015b). A strong focus of this instrumental setup  
556 | is to gain insight into the relationships between ground surface reflectance and savanna ecosystem  
557 | properties for EO up-scaling purposes. This paper presents a unique in situ dataset of seasonal  
558 | dynamics in hyperspectral [reflectanceHCRF](#) and demonstrates how ~~seasonal dynamics in hyperspectral~~  
559 | ~~reflectanceit~~ can be used to describe the seasonal dynamics in ecosystem properties of semi-arid  
560 | savanna ecosystems. The objectives are threefold: (i) to quantify the relationship between seasonal  
561 | dynamics of in situ hyperspectral [reflectanceHCRF](#) between 350 and 1800 nm and ecosystem  
562 | properties (biomass, gross primary productivity (GPP), LUE, and FAPAR); (ii) to quantify the  
563 | relationship between NDSI with different wavelength combinations (350 to 1800 nm) and the  
564 | measured ecosystem properties; (iii) to analyse and quantify effects of variable sun angles and sensor  
565 | viewing geometries on different NDSI combinations.

## 566 | **2. Materials and Method**

### 567 | **2.1 Site description**

568 | All measurements used for the present study were conducted at the Dahra field site in the Sahelian  
569 | ecoclimatic zone north-east of the town Dahra in the semi-arid central part of Senegal (15°24'10"N,

570 | 15°25'56"W) during 2011 and 2012 (Fig. 1). Rainfall is sparse in the region with a mean annual sum of  
571 | 416 mm (1951-2003). More than 95% of the rain falls between July and October, with August being  
572 | the wettest month. The mean annual air temperature is 29 °C (1951-2003), May is the warmest and  
573 | January is the coldest month with mean monthly temperature of 32°C and 25°C, respectively. The  
574 | Dahra site has a short growing season (~3 months), following the rainy season with leaf area index  
575 | generally ranging between 0 and 2 (Fensholt et al., 2004). South-western winds dominate during the  
576 | rainy season and north-eastern winds dominate during the dry season. The area is dominated by annual  
577 | grasses (e.g. *Schoenefeldia gracilis*, *Digitaria gayana*, *Dactyloctenium aegypticum*, *Aristida mutabilis*  
578 | and *Cenchrus biflorus*) (Mbow et al., 2013) and trees and shrubs (e.g. *Acacia senegalensis* and  
579 | *Balanites aegyptiaca*) are relatively sparse (~3% of the land cover) (Rasmussen et al., 2011). The  
580 | average tree height was 5.2 m and the peak height of the herbaceous layer was 0.7 m (Tagesson et al.,  
581 | 2015b). A thorough description of the Dahra field site is given in Tagesson et al. (2015b).  
582 | <Figure 1>

## 583 | 2.2 Meteorological and vegetation variables

584 | ~~At the Dahra field site, a~~ range of meteorological variables have been measured ~~from~~ a tower at the  
585 | Dahra field site for more than ten years in a tower located at a for more than ten years ~~sunlit grass~~  
586 | patch: air temperature (°C) and relative humidity (%) were measured at 2 m height; soil temperature  
587 | (°C) and soil moisture (volumetric water content ( $\text{m}^3 \text{m}^{-3} \times 100$ ) (%)) were collected at 0.05m depths;  
588 | rainfall (mm) was measured at 2 m height; incoming ( $_{inc}$ ) and reflected ( $_{ref}$ ) PAR ( $\mu\text{mol m}^{-2} \text{s}^{-1}$ ) was  
589 | measured at 10.5 m height, and PAR transmitted through the vegetation ( $\text{PAR}_{transmit}$ ) was measured at 6  
590 | plots at ~0.01 m height (Table 1) (Tagesson et al., 2015b). The  $\text{PAR}_{transmit}$  was measured within 7  
591 | meters distance from the tower. PAR absorbed by the vegetation (APAR) was estimated by:

592 
$$APAR = PAR_{inc} - PAR_{ref} - (1 - \alpha_{soil}) \times PAR_{transmit} \quad (1)$$

593 where  $\alpha_{soil}$  is the PAR albedo of the soil, which was measured as 0.20 (Tagesson et al., 2015b). ~~and~~

594 FAPAR was estimated by dividing APAR with  $PAR_{inc}$  (Tagesson et al., 2015b). All sensors were

595 connected to a CR-1000 logger in combination with a multiplexer (Campbell Scientific Inc., North

596 Logan, USA) and data were sampled every 30 s, and stored as 15 minute averages (sum for rainfall).

597 The total above ground green biomass ( $g\ m^{-2}$ ) of the ~~grass and~~ herbaceous vegetation was sampled

598 approximately every 10 days during the growing seasons 2011 and 2012 at 28 one  $m^2$  plots located

599 along two ~1060 m long diagonal transects (Fig. 1f) (Mbow et al., 2013). The method applied was

600 destructive, so even though the same transects were used for each sampling date, the plots were never

601 located positioned at exactly the same location. The study area is flat and characterised by homogenous

602 grassland savanna and the conditions in these sample plots are generally found to be representative for

603 the conditions in the entire measurement area (Fensholt et al., 2006). All above ground green ~~grass and~~

604 herbaceous vegetation matter was collected and weighed in the field to get the fresh weight. The dry

605 matter (DW) was estimated by oven-drying the green biomass. For a thorough description regarding

606 the biomass sampling we refer to Mbow et al. (2013).

607 <Table 1>

608

### 609 **2.3 Estimates of gross primary productivity and light use efficiency**

610 Net ecosystem exchange of  $CO_2$  (NEE) ( $\mu mol\ CO_2\ m^{-2}\ s^{-1}$ ) was measured with an eddy covariance

611 system, consisting of an open path infrared gas analyser (LI-7500, LI-COR Inc., Lincoln, USA) and a

612 3-axis sonic anemometer (~~GILL-Gill~~ instruments, Hampshire, UK) from 18 July 2011 until 31

613 December 2012. (Table 1). The sensors were mounted 9 m above the ground on a tower (~~located placed~~

614 50 m south of the tower containing including the meteorological and spectroradiometric sensors) (Fig.  
615 1f). Data were sampled at 20 Hz rate. The post-processing was done with the EddyPro 4.2.1  
616 software (LI-COR Biosciences, 2012), and the statistics were calculated for 30 minute periods. The  
617 post-processing includes 2-D coordinate rotation (Wilczak et al., 2001), time lag removal between  
618 anemometer and gas analyser by covariance maximization (Fan et al., 1990), despiking (Vickers and  
619 Mahrt, 1997) (plausibility range: window average  $\pm 3.5$  standard deviations), linear detrending  
620 (Moncrieff et al., 2004), and compensation for density fluctuations (Webb et al., 1980). The fluxes  
621 were also corrected for high pass (Moncrieff et al., 1997) and low pass filtering effects (Moncrieff et  
622 al., 2004). The data were filtered for steady state and fully developed turbulent conditions, following  
623 Foken et al. (2004), and according to statistical tests as recommended by Vickers and Mahrt (1997).  
624 Flux measurements from periods of heavy rainfall were also removed. For a thorough description of the  
625 post processing of the raw eddy covariance data, see Tagesson et al. (2015a).  
626 A possible source of error in a comparison between EC-based variables and spectral  
627 reflectance HCRF is the difference in footprint/ instantaneous field of view (IFOV) differences  
628 between the sensors. The IFOV of the spectroradiometer set-up contains only the including soil and  
629 herbaceous vegetation. The footprint of the EC tower was estimated using a model based on  
630 measurement height, surface roughness and atmospheric stability (Hsieh et al., 2000). The median  
631 point of maximum contribution is at 69 m, and the median for 70% cumulative flux distance is at 388  
632 m from the tower. The footprint of the EC tower contains semi-arid savanna grassland with ~3% tree  
633 coverage and the EC data is thereby affected by both woody and herbaceous vegetation (Fig. 1a and  
634 1f). But given the low tree coverage, and the dominant influence of herbaceous vegetation on the  
635 seasonal dynamics in CO<sub>2</sub> fluxes, we still consider it reasonable to compare EC fluxes with seasonal  
636 dynamics in spectral HCRF of the herbaceous vegetation.

637 The daytime NEE was partitioned to GPP and ecosystem respiration using the Mitscherlich light  
 638 response function against PAR<sub>inc</sub> (Falge et al., 2001). A 7-day moving window with one day time steps  
 639 was used when fitting the functions. By subtracting dark respiration (R<sub>d</sub>) from the light response  
 640 function, it was forced through 0, and GPP was estimated:

$$641 \quad GPP = -(F_{\text{csat}} + R_d) \times \left(1 - e^{\left(\frac{-\alpha \times \text{PAR}_{\text{inc}}}{F_{\text{csat}} + R_d}\right)}\right) \quad (32)$$

642 where F<sub>csat</sub> is the CO<sub>2</sub> uptake at light saturation (μmol CO<sub>2</sub> m<sup>-2</sup> s<sup>-1</sup>), and α is the quantum efficiency or  
 643 the initial slope of the light response curve (μmol CO<sub>2</sub> (μmol photons)<sup>-1</sup>) (Falge et al., 2001). Vapor  
 644 pressure deficit (VPD) limits GPP and to account for this effect, the F<sub>csat</sub> parameter was set as an  
 645 exponentially decreasing function:

$$646 \quad F_{\text{csat}} = \begin{cases} F_{\text{csat}} \times e^{-k(\text{VPD} - \text{VPD}_0)} & \text{VPD} > \text{VPD}_0 \\ F_{\text{csat}} & \text{VPD} < \text{VPD}_0 \end{cases} \quad (43)$$

647 where VPD<sub>0</sub> is 10 hPa following the method by Lasslop et al. (2010).

648 Gaps in GPP less or equal to three days were filled with three different methods: (i) gaps shorter than  
 649 two hours were filled using linear interpolation; (ii) daytime gaps were filled by using the light-  
 650 response function for the 7-day moving windows; (iii) remaining gaps were filled by using mean  
 651 diurnal variation 7-days moving windows (Falge et al., 2001). A linear regression model was fitted  
 652 between daytime GPP and APAR for each 7-day moving window to estimate LUE, where LUE is the  
 653 slope of the line.

## 654 2.4 Hyperspectral reflectanceHCRF measurements and NDSI estimates

655 Ground surface reflectanceHCRF spectra were measured every 15 minutes between sunrise and sunset  
 656 from 15 July 2011 until 31 December 2012 using two FieldSpec3 spectrometers with fiber optic cables  
 657 (Table 1) (ASD Inc., Colorado, USA). The spectroradiometers cover the spectral range from 350 nm to

658 1800 nm and have an ~~instantaneous field of view~~FOV of 25°. The spectral resolution is 3 nm at 350-  
659 1000 nm and 10 nm at 1000-1800 nm and the sampling interval is 1.4 nm at 350-1000 nm and 2 nm at  
660 1000-1800 nm. From these data, 1 nm spectra were calculated by using cubic spline interpolation  
661 functions. One sensor head was mounted on a rotating head 10.5 m above the surface (~~at~~ the same  
662 tower containing ~~including instruments to measure~~ the measurements of meteorological variables)  
663 providing measurements ~~from of the land surface~~ a sunlit grass patch ~~the herbaceous vegetation from~~  
664 seven different viewing angles in a transect underneath the tower (nadir, 15°, 30°, 45° off-nadir angles  
665 towards east and west). ~~There are n~~ No trees or effects of shading of trees are present in the HFOV of  
666 the data used in this study (Fig. 1). A reflective cosine receptor is used to measure full-sky-irradiance;  
667 ~~it constitutes of by having t~~ The second sensor head was mounted on a 2 m high stand pointing to a  
668 Spectralon panel (Labsphere Inc., New Hampshire, USA) under a glass dome. ~~used for full-sky-~~  
669 ~~irradiance measurements.~~  
670 Each sensor measurement starts with an optimization to adjust the sensitivity of the detectors  
671 according to the specific illumination conditions at the time of measurement. The optimisation is  
672 followed by a dark current measurement to account for the noise generated by the thermal electrons  
673 within the ASDs that flows even when no photons are entering the device. The measurement sequence  
674 starts with a full-sky-irradiance measurement, secondly followed by measurements from of the 7  
675 angles of the land surface is conducted, and finally by a second full-sky-irradiance is  
676 measurement. Thirty scans are averaged to one measurement to improve the signal-to-noise ratio for  
677 each measurement (optimisation, dark current, full-sky irradiance and each of the seven target  
678 measurements). The full measurement sequence takes less than one minute. The two ASD instruments  
679 are calibrated against each other before and after each rainy season. Poor quality measurements caused



680 by unfavorable weather conditions, changing illumination conditions, irregular technical issues were  
681 filtered by comparing full-sky solar irradiance before and after the target measurements (Huber et al.,  
682 2014). The spectral reflectanceHCRF was derived by estimating the ratio between the ground surface  
683 radiance and full sky irradiance. For a complete description/illustration of the spectroradiometer set up,  
684 the measurement sequence and the quality control, see Huber et al. (2014).

685 NDSI using all possible combinations of two separate wavelengths were calculated as:

$$686 \quad \text{NDSI} = \frac{(\rho_i - \rho_j)}{(\rho_i + \rho_j)} \quad (54)$$

687 where  $\rho_i$  and  $\rho_j$  are the daily median reflectanceHCRF in two separate single wavelengths ( $i$  and  $j$ )  
688 between 350 and 1800 nm. In order to minimise the influence of errors we used daily median  
689 hyperspectral HCRF in the analysis (since median provides the most common model output and is  
690 thereby more robust against outliers than average values). ~~Additionally, NDSI including the water~~  
691 absorption band (1300-1500 nm) was filtered as it is strongly sensitive to atmospheric water content,  
692 and is less suitable for spatial extrapolation of ecosystem properties using air/space borne sensors  
693 (Asner, 1998). Finally, NDSI combinations including wavelengths between 350 and 390 nm were  
694 filtered owing to low signal to noise ratio in the ASD sensors (Thenkabail et al., 2004).

## 695 **2.5 Effects of varying sun and sensor viewing geometry on NDSI**

696 The effects of variable solar zenith angles on different NDSI combinations were studied with nadir  
697 measurements taken over 15 days during the peak of the growing season in 2011 (day of year 237-251).  
698 Only days with full data coverage were used (12 of the 15 days) in order not to include bias in the  
699 results from days with incomplete datasets. The median reflectanceHCRF of the 15 days was calculated  
700 for each wavelength for every 15 minutes between 8:00 and 18:00. These reflectanceHCRF values

701 were combined into NDSI with different wavelength combinations. Finally, daily mean and standard  
 702 deviation for all wavelength combinations were calculated. Diurnal variability in the NDSI was  
 703 assessed with the coefficient of variation (COV), which is the ratio between the standard deviation and  
 704 the mean. The COV gives an indication of effects related to variable solar zenith angles.

705 To capture directional effects in the NDSI related to the variable view zenith angles (15°, 30°, 45°  
 706 off-nadir angles towards east and west) the NDSI was calculated using median HCRF values from the  
 707 peak of the growing season 2011 (day of year 237-251) for the different viewing angles. Only data  
 708 measured between 12:00 and 14:00 was used to avoid effects of variable solar zenith angles. The  
 709 anisotropy factor (ANIF)~~The anisotropy factor (ANIF) was used to capture directional effects in the~~  
 710 ~~NDSI related to the variable view zenith angles (15°, 30°, 45° off nadir angles towards east and west).~~  
 711 ~~The ANIF~~ is defined as the fraction of a reflected property at a specific view direction relative to the  
 712 nadir, and it was calculated by:

713 
$$\text{ANIF}(\lambda, \theta) = \frac{\text{NDSI}(\lambda, \theta)}{\text{NDSI}_0(\lambda)} \quad \text{---} \quad (65)$$

714 where  $\text{NDSI}(\lambda, \theta)$  is NDSI for the different wavelengths ( $\lambda$ ) and the different viewing angles ( $\theta$ ), and  
 715  $\text{NDSI}_0(\lambda)$  is the nadir measured NDSI (Sandmeier et al., 1998). ~~The NDSI was calculated from median~~  
 716 ~~reflectance~~HCRF values from the peak of the growing season 2011 (day of year 237-251) and only data  
 717 ~~measured between 12:00 and 14:00 were used to avoid effects of variable solar zenith angles.~~

718 **2.6 Relationship between hyperspectral reflectanceHCRF, NDSI and ecosystem**  
 719 **properties**

720 We examined the relationship between predictor variables (daily median hyperspectral  
 721 reflectanceHCRF, and NDSI from nadir observations) and response variables (biomass, GPP, LUE, and  
 722 FAPAR) using linear regression analysis. There are pPossible errors (random sampling errors, weather

723 ~~conditions, aerosols, dust or water on the sensor heads, electrical sensor noise, filtering and gap-filling~~  
724 ~~errors, errors in correction factors, sensor drift, and instrumentation errors) can be present in both~~  
725 ~~predictor and response variables~~HCRF~~(provides is ther)~~. We ~~thereby~~ used a reduced major axis linear  
726 regression to account for errors in both the predictor and response variables ~~when fitting the regression~~  
727 ~~lines~~. In order to estimate the robustness of the empirical relationships, we used a bootstrap simulation  
728 methodology, where the datasets were copied 200 times (Richter et al., 2012). The runs generated 200  
729 sets of slopes, intercepts, coefficients of determination ( $R^2$ ), ~~and root-mean-square errors (RMSE)~~,  
730 from which median and standard deviation was estimated. ~~The generated statistical models were~~  
731 ~~validated against the left-out subsamples within the bootstrap simulation method by calculating the~~  
732 ~~root-mean square error (RMSE) and the relative RMSE ( $RRMSE=100*RMSE*\text{mean}(\text{observed})^{-1}$ );~~  
733 ~~median and standard deviation~~ ~~was~~~~were~~ estimated. ~~Median was used instead of average since it gives~~  
734 ~~the most common model output and hereby more robust against outliers~~. Within the regression analysis  
735 all variables used were repeated observations of the same measurement plot. The dependent and  
736 independent variables are thereby temporally auto-correlated and cannot be regarded as statistically  
737 independent. We thereby choose not to present any statistical significance. The analyses, however, still  
738 indicate how closely coupled the explanatory variables are with the ecosystem properties.

739 A filter was created for the analysis between NDSI and ecosystem properties; all NDSI combinations  
740 with a COV higher than 0.066 and all NDSI combinations with ANIF values higher than 1.2 and lower  
741 than 0.8 were filtered. ~~The ANIF threshold of 1.2 and 0.8, and t~~The COV threshold of 0.066 was used  
742 since ~~99.9% of the~~ values ~~then~~ vary less than 20% due to effects of variable ~~sun-sensor geometrysolar~~  
743 ~~zenith angles. Additionally, the water absorption band (1300-1500 nm) was filtered as it is strongly~~  
744 ~~sensitive to atmospheric water content, and is less suitable for spatial extrapolation of ecosystem~~  
745 ~~properties using air/space borne sensors (Asner, 1998). Finally, NDSI combinations including~~

746 | ~~wavelengths between 350 and 390 nm were filtered owing to low signal to noise ratio in the ASD~~  
747 | ~~sensors (Thenkabail et al., 2004).~~

### 748 | 3. Results

#### 749 | 3.1 Seasonal dynamics in meteorological variables, ecosystem properties and 750 | hyperspectral [reflectanceHCRF](#)

751 | Daily average air temperature at 2 m height ranged between 18.4°C and 37.8°C, with low values during  
752 | winter and peak values ~~in-at~~ the end of the dry season (Fig. 2a). Yearly rainfall was 486 mm and 606  
753 | mm for 2011 and 2012, respectively. Soil moisture ranged between 1.9% and 14.1%, and it clearly  
754 | followed the rainfall patterns (Fig. 2b and 2c). The CO<sub>2</sub> fluxes were low during the dry period and high  
755 | during the rainy season (July-October) (Fig. 2e). The LUE followed GPP closely (Fig. 2f). FAPAR was  
756 | low at the start of the rainy season, followed by a maximum towards the end of the rainy season, and  
757 | then slowly decreased over the dry season (Fig. 2g).

758 | The range in [reflectanceHCRF](#) is large across the spectral space, and would hide the seasonal  
759 | dynamics in hyperspectral [reflectanceHCRF](#) if directly shown. Therefore, to clearly illustrate the  
760 | seasonal dynamics in hyperspectral [reflectanceHCRF](#), the ratio between daily median nadir  
761 | [reflectanceHCRF](#) and the average [reflectanceHCRF](#) for the entire measurement period was calculated  
762 | for each wavelength (350-1800 nm). This gives a fraction of how the [reflectanceHCRF](#) for each  
763 | wavelength varies over the measurement period in relation to the average of the entire period (Fig. 2d).  
764 | In the visible (VIS) part of the [reflectance](#)-spectrum (350-700 nm) there was a stronger absorption  
765 | during the second half of the rainy season and at the beginning of the dry season than during the main  
766 | part of the dry season and the start of the rainy season. There was stronger NIR absorption (700-1300  
767 | nm) ~~in-at~~ the end of the rainy season and the beginning of the dry season, whereas the absorption  
768 | decreased along with the dry season. Strong seasonal variation was observed in the water absorption

769 | region around 1400 nm following the succession of rainy and dry seasons. [ReflectanceHCRF](#) in the  
770 short-wave infrared (SWIR; 1400-1800 nm) generally followed the seasonal dynamics of the visible  
771 part of the spectrum.

772 <Figure 2>

### 773 **3.2 Effects of sensor viewing geometry and variable sun angles on NDSI**

774 The most pronounced effects of solar zenith angles at the peak of the growing season 2011 were  
775 observed for NDSI combining SWIR and NIR wavelengths, and with VIS wavelengths between 550  
776 nm and 700 nm (n=576) (Fig. 3). Remaining VIS wavelengths were mostly affected by solar zenith  
777 angles when combined with the water absorption wavelengths around 1400 nm. The same effects were  
778 seen for the view zenith angles; the strongest effects were seen for NDSI with SWIR and NIR  
779 combinations, and VIS wavelengths between 550 and 700 nm (Fig. 4). Remaining VIS wavelengths  
780 were less affected. It was also clear that ground surface anisotropy increased strongly as a function of  
781 increasing viewing angle (Fig. 4). Moreover, some band combinations showed already angular  
782 sensitivity at view zenith angles of 15 °, while other band combinations only manifest anisotropic  
783 behaviour with higher view angles. Some band combinations, however, do not show any increased  
784 anisotropy at all (areas coloured in green in all three plots).

785 <Figure 3>

786 <Figure 4>

787 **3.3 Relationship between hyperspectral reflectanceHCRF, NDSI and ecosystem**  
788 **properties**

789 **3.3.1 Biomass**

790 ReflectanceHCRF values for all wavelengths except the water absorption band at 1100 nm were  
791 strongly correlated to biomass (Fig. 5a). The strongest correlation was found at  $\rho_{1675}$  (median  $\pm$  1  
792 standard deviation;  $r = -0.88 \pm 0.09$ ), but biomass was almost equally well correlated to blue, red and  
793 NIR wavelengths. All presented correlations and relationships throughout the text are based on  
794 filtered data. Negative correlations indicate that the more biomass the higher the absorption and hence  
795 the lower the reflectanceHCRF. A small peak of positive correlation is seen at 1120-1150 nm caused  
796 by a water absorption peak around this wavelength (Thenkabail et al., 2012).  
797 – NDSI combinations with reflectanceHCRF in the red edge ( $\rho_{680}-\rho_{750}$ ) and reflectanceHCRF in the  
798 VIS region explained seasonal dynamics in biomass well (Fig. 6a). The strongest relationship  
799 ( $R^2 = 0.88 \pm 0.07$ ; RRMSE = 28.418.6  $\pm$  85.7 % g-DW m<sup>-2</sup>) between NDSI and biomass was found for  
800 NDSI combining 705 and 587 nm (NDSI[705, 587]) (Table 42, Fig. 7a).

801 **3.3.2 Gross primary productivity**

802 The relationship between GPP and nadir measured hyperspectral reflectanceHCRF is inverted as  
803 compared to other correlation coefficient lines (Fig. 5b), since GPP is defined as a withdrawal of CO<sub>2</sub>  
804 from the atmosphere with higher negative values for a larger CO<sub>2</sub> uptake. The seasonal dynamics in  
805 GPP was strongly positively correlated to reflectanceHCRF in the blue, red, SWIR wavelengths, and  
806 the water absorption band at 1100 nm whereas it was strongly negatively correlated to the NIR  
807 reflectanceHCRF. The study revealed the strongest positive and negative correlations for  
808 reflectanceHCRF at 682 nm ( $r = -0.70 \pm 0.02$ ) and 761 nm ( $r = -0.74 \pm 0.02$ ), respectively. NDSI  
809 combinations that explained most of the GPP variability were different combinations of the VIS and

810 NIR or red and SWIR wavelengths (Fig. 6b). However, the strongest relationship was seen at  
811 NDSI[518, 556] ( $R^2=0.86\pm0.02$ ;  $\underline{RRMSE=1.534.9\pm0.12.3\%g\ C\ m^{-2}\ d^{-1}}$ ) (Table 42; Fig. 7b).

### 812 3.3.3 Light use efficiency

813 LUE was negatively correlated with [reflectanceHCRF](#) in the blue, and red spectral ranges and in the  
814 water absorption band at 1100 nm and it was positively correlated in the NIR wavelengths (Fig. 5c).  
815 [ReflectanceHCRF](#) at 761 nm yielded the strongest positive correlation ( $r=-0.87\pm0.01$ ). When  
816 combining the different wavelengths to NDSI, the VIS wavelengths explained variation in LUE well,  
817 with the strongest relationships in the red and blue parts of the spectrum (Fig. 6c). LUE correlated most  
818 strongly with NDSI[436, 688] ( $R^2=-0.81\pm0.02$ ;  $\underline{RRMSE=0.2652.8\pm0.023.8\%g\ C\ MJ^{-1}}$ ) (Table 42;  
819 Fig. 7c).

### 820 3.3.4 Fraction of photosynthetically active radiation absorbed by the vegetation

821 FAPAR was negatively correlated to nadir measured [reflectanceHCRF](#) for most wavelengths (Fig. 5d);  
822 the higher FAPAR the higher the absorption, and thereby the lower the [reflectanceHCRF](#). The strongest  
823 correlation was found at a blue wavelength  $\rho_{412}$  ( $r=-0.92\pm0.01$ ). When wavelengths were combined to  
824 NDSI, combining violet/blue with NIR and SWIR wavelengths generated the NDSI with the strongest  
825 relationships (Fig. 6d) with a maximum  $R^2$  of  $0.81\pm0.02$  ( $\underline{RRMSE=0.05914.6\pm0.0030.7\%}$ ) for  
826 NDSI[399, 1295] (Table 42; Fig. 7d).

827 <Table 42>

828 <Figure 5>

829 <Figure 6>

830 <Figure 7>

## 831 4. Discussion

### 832 4.1 Effects of sensor viewing geometry and variable sun angles on the NDSI

833 Effects of solar zenith angles and sensor viewing geometry were similar (Fig. 3 and 4), since they  
834 affect [reflectanceHCRF](#) measurements in a similar way (Kimes, 1983). In dense and erectophile  
835 canopies, [reflectanceHCRF](#) increases with sensor viewing and solar zenith angles, because a larger  
836 fraction of the upper vegetation canopy is viewed/illuminated, whereas the shadowed lower part of the  
837 canopy contributes less to the measured signal as shown previously by several studies (Huete et al.,  
838 1992; Jin et al., 2002; Huber et al., 2014; Kimes, 1983). However, the radiative transfer within a green  
839 canopy is complex, and differs across the spectral region (Huber et al., 2014). Less radiation is  
840 available for scattering of high absorbing spectral ranges (such as the VIS wavelengths), and this tends  
841 to increase the contrast between shadowed and illuminated areas for these wavelengths, whereas in the  
842 NIR and SWIR ranges, more radiation is scattered and transmitted, which thereby decreases the  
843 difference between shadowed and illuminated areas within the canopy (Kimes, 1983; Hapke et al.,  
844 1996). A recognised advantage of NDSI calculations is that errors/biases being similar in both  
845 wavelengths included in the index are suppressed by the normalisation. However, for a given situation  
846 where errors/biases are different for the wavelengths used, such as effects generated by sun-sensor  
847 geometry, it will affect the value of the index. This was also the case at the Dahra field site: NDSI  
848 values were strongly affected at wavelength combinations with large differences in effects of variable  
849 solar zenith angles (Fig. 6 in Huber et al. (2014)) and at wavelength combinations with large  
850 differences in effects related to the variable view zenith angles (Fig. 4 in Tagesson et al. (2015b)). This  
851 effect is especially pronounced in the case for low index values (closer to 0) whereas larger index  
852 values (closer to 1 and -1) become less sensitive. The relative [reflectanceHCRF](#) difference between  
853 NIR and SWIR is lower as compared to indices including the VIS domain; NIR/SWIR based indices



854 thereby generate lower NDSI values with higher sensitivity to sun-sensor geometry generated  
855 differences between included wavelengths (Fig. 3 and 4).

856 The importance of directional effects for the applicability of normalized difference spectral indices  
857 has been pointed out as an issue in numerous papers (e.g. Holben and Fraser, 1984; van Leeuwen et al.,  
858 1999; Cihlar et al., 1994; Fensholt et al., 2010; Gao et al., 2002). This study confirms these challenges  
859 for NIR/SWIR based indices, but the results also indicate several wavelength combinations from which  
860 these effects are less severe and potentially applicable to EO data without disturbance from  
861 viewing/illumination geometry for this type of vegetation. ~~Additionally, M-multi-angular~~  
862 ~~reflectance~~HCRF data provide ~~accurate and extra~~additional information of e.g. canopy structure,  
863 photosynthetic efficiency and capacity (Bicheron and Leroy, 2000; Asner, 1998; Pisek et al., 2013),  
864 and this unique in situ based multi-angular high temporal resolution dataset may thus be used for future  
865 research of canopy radiative transfer ~~and creation, parameterisation and evaluation of BRDF~~  
866 ~~(bidirectional reflectance distribution functions)~~ modelling (Jacquemoud et al., 2009; Bicheron and  
867 Leroy, 2000). The multi-angular dataset is also highly valuable for evaluation and validation of satellite  
868 based products, where the separation of view angle and atmospheric effects can only be done using  
869 radiative transfer models (Holben and Fraser, 1984).

## 870 **4.2 Seasonal dynamics in hyperspectral ~~reflectance~~HCRF, NDSI and ecosystem** 871 **properties**

### 872 **4.2.1 Biomass**

873 The strong correlation between biomass and ~~the majority-most~~ of the ~~reflectance~~spectrum indicates the  
874 strong effects of phenology on the seasonal dynamics in the ~~reflectance~~HCRF spectra (Fig. 5a).  
875 Variability in VIS (350-700 nm) ~~reflectance~~HCRF for vegetated areas is strongly related to changes in  
876 leaf pigments (Asner, 1998), and this can also be seen in Fig. 2d since absorption was much stronger

877 during the rainy (growing) season, than during the dry season. Previous studies have generally shown  
878 positive relationships between NIR reflectanceHCRF and biomass since ~~To avoid overheating~~ a large  
879 fraction of NIR radiation is reflected in green healthy vegetation to avoid overheating and NIR  
880 reflectance is mostly affected by changes in LAI, canopy architecture, and by the spongy mesophyll  
881 layer in green leaves (e.g. Hansen and Schjoerring, 2003; Asner, 1998). ~~(e.g. Hansen and Schjoerring,~~  
882 ~~2003)~~ Here, We a generally showed strong negative relationships between NIR HCRF and dry weight  
883 biomass is generally observed (Fig. 5a), whereas a being very different from a strong positive NIR  
884 HCRF correlation with vegetation water content was seen (figure not shown). an increased  
885 from within HCRF general conditions ~~The strong negative NIR HCRF correlation with dry weight~~  
886 biomass found here This is interesting and should be studied further to better understand the respective  
887 importance of canopy water and leaf internal cellular structure for the NIR HCRF of herbaceous  
888 vegetation characterised by erectophile leaf angle distribution (LAD). ~~Several studies have shown that~~  
889 ~~biomass accumulation increases ecosystem water content, which thereby increases SWIR absorption~~  
890 ~~(e.g. Psomas et al., 2011; Asner, 1998).~~ We found the strongest correlation for biomass with a SWIR  
891 wavelength thereby confirming the studies by Lee (2004) and Psomas et al. (2011) in that SWIR  
892 wavelengths are good predictors of LAI or biomass.

893 The NDVI is known to saturate at high biomass because the absorption of red light at ~670-680 nm  
894 reaches a peak saturates at higher biomass loads whereas the NIR reflectanceHCRF continues to  
895 increase due to multiple scattering effects (Mutanga and Skidmore, 2004; Jin and Eklundh, 2014).  
896 Several studies have shown that NDSI computed with narrowband reflectanceHCRF improve this  
897 relationship by choosing a wavelength region not as close to the maximum red absorption at ~680 nm,  
898 for example using shorter and longer wavelengths of the red edge (700 - 780nm) (Cho et al., 2007;  
899 Mutanga and Skidmore, 2004; Lee, 2004), and NIR and SWIR wavelengths (Psomas et al., 2011; Lee,

900 2004). The NDSI with the strongest correlation to biomass was computed using red edge  
901 [reflectanceHCRF](#) ( $\rho_{705}$ ) and green [reflectanceHCRF](#) ( $\rho_{587}$ ). Vegetation stress and information about  
902 chlorophyll and nitrogen status of plants can be extracted from the red-edge region (Gitelson et al.,  
903 1996).- Wavelengths around  $\rho_{550}$  are located right at the peak of green reflection and closely related to  
904 the total chlorophyll content, leaf nitrogen content,- and chlorophyll/carotenoid ratio and have  
905 previously been shown to be closely related to biomass (Inoue et al., 2008; Thenkabail et al., 2012).

#### 906 **4.2.2 Gross primary productivity**

907 The maximum absorption in the red wavelengths generally occurs at 682 nm as this is the peak  
908 absorption for chlorophyll a and b (Thenkabail et al., 2000), and this was also the wavelength being  
909 most strongly correlated with GPP. [ReflectanceHCRF](#) at 682 nm was previously shown to be strongly  
910 related to LAI, biomass, plant height, NPP, and crop type discrimination (Thenkabail et al., 2004;  
911 Thenkabail et al., 2012). The NDSI with the strongest relationship to GPP was based on  
912 [reflectanceHCRF](#) in the vicinity of the green peak. The photochemical reflectance index (PRI)  
913 normalizes [reflectanceHCRF](#) at 531 nm and 570 nm and it was suggested for detection of diurnal  
914 variation in the xanthophyll cycle activity (Gamon et al., 1992), and it is commonly used for estimating  
915 productivity efficiency of the vegetation (e.g. Soudani et al., 2014). The present study thereby confirms  
916 the strong applicability of the wavelengths in the vicinity of the green peak for vegetation productivity  
917 studies. Again, wavelengths around the green peak are related to the total chlorophyll content, leaf  
918 nitrogen content, chlorophyll/carotenoid ratio, and biomass (Inoue et al., 2008; Thenkabail et al., 2012).

#### 919 **4.2.3 Light use efficiency**

920 Both LUE and GPP were most strongly correlated with [reflectanceHCRF](#) at 761 nm, which is the  
921 oxygen A-band within the NIR wavelengths. [ReflectanceHCRF](#) at 761 nm is commonly used for

922 estimating solar-induced chlorophyll fluorescence due to radiation emitted by the chlorophyll, and it  
923 has been suggested as a direct measure of health status of the vegetation (Meroni et al., 2009). ~~As~~  
924 ~~fluorescence is competing with photochemical conversion, it may allow a more correct estimate of the~~  
925 ~~carbon assimilation (Entcheva Campbell et al., 2008).~~ Earth observation data for estimating  
926 fluorescence should have very high spectral resolution (~~<10 nm~~) (~~0.05–0.1 nm~~) due to its narrow  
927 features, but considering the rapid technical development within sensors for hyperspectral  
928 measurements, fluorescence possibly has strong practical potential for monitoring vegetation status  
929 (Meroni et al., 2009; Entcheva Campbell et al., 2008). Globally mapped terrestrial chlorophyll  
930 fluorescence retrievals are already produced from the GOME-2 instrument at a spatial resolution of  
931  $0.5^{\circ} \times 0.5^{\circ}$ , but hopefully this will be available also with EO sensors of higher spatial and temporal  
932 resolution in the future (Joiner et al., 2013).

933 The strongest wavelength combinations for estimating LUE for this semi-arid ecosystem was  
934 NDSI[688, 435]. The 688 nm wavelength is just at the base of the red edge region, again indicating the  
935 importance of this spectral region for estimating photosynthetic activity. The wavelength at 435 nm is  
936 at the center of the blue range characterized by chlorophyll utilization, and strongly related to  
937 chlorophyll a and b, senescing, carotenoid, loss of chlorophyll, and vegetation browning (Thenkabail et  
938 al., 2004; Thenkabail et al., 2012). The NDSI[688, 435] thereby explores the difference between  
939 information about chlorophyll content and information about senescence of the ~~vegetation canopy~~,  
940 which should be a good predictor of ecosystem level photosynthetic efficiency.

#### 941 **4.2.4 Fraction of photosynthetically active radiation absorbed by the vegetationFAPAR**

942 FAPAR is an estimate of radiation absorption in the photosynthetically active spectrum and thereby  
943 strongly negatively correlated to most parts of the ~~reflectance~~ spectrum (Fig. 5d). FAPAR remained

944 high during the dry season because of standing dry biomass that was slowly degrading over the dry  
945 season (Fig. 2g). The seasonal dynamics in FAPAR is thereby strongly related to senescence of the  
946 vegetation, which explains why FAPAR was most strongly correlated to blue wavelengths ( $\rho_{412}$ ).  
947 Several studies reported a strong relationship between NDVI and FAPAR (e.g. Tagesson et al., 2012;  
948 Myneni and Williams, 1994; Fensholt et al., 2004), but this relationship has been shown to vary for the  
949 vegetative phase and the periods of senescence (Inoue et al., 1998; Tagesson et al., 2015b). As showed  
950 by Inoue et al. (2008), and confirmed by this study, new indices combining blue with NIR wavelengths  
951 could be used for estimating FAPAR for the entire phenological cycle. This result has implications for  
952 studies using the LUE approach for estimating C assimilations (Hilker et al., 2008).

### 953 **4.3 Outlook and perspectives**

954 Very limited multi-angular hyperspectral in situ data exists, even though it has been, and will continue  
955 to be extremely valuable for an improved understanding of the interaction between ground surface  
956 properties and radiative transfer. In this study, we have presented a unique in situ dataset of multi-  
957 angular, high temporal resolution hyperspectral [reflectanceHCRF](#) (350-1800 nm) and demonstrated the  
958 applicability of hyperspectral data for estimating ground surface properties of semi-arid savanna  
959 ecosystems using NDSI. The study was conducted in spatially homogeneous savanna grassland,  
960 suggesting that the results should be commonly applicable for this biome type. However, attention  
961 should be paid to site-specific details that could affect the indices, such as species composition, soil  
962 type, biotic and abiotic stresses, and stand structure. Additionally, the biophysical mechanisms behind  
963 the NDSIs are not well understood at the moment, and further studies are needed to examine the  
964 applicability of these indices to larger regions and other ecosystems. Being a 2-band ratio approach,  
965 NDSI does not take full advantage of exploring the rich information given by the hyperspectral

966 | [reflectanceHCRF](#) measurements. In the future, this hyperspectral [reflectanceHCRF](#) data-set could be  
967 | fully explored using e.g. derivative techniques, multivariate methods, and creation, parameterisation  
968 | and evaluation of [bidirectional reflectance distribution functionsBRDF](#) and radiative transfer models.  
969 | Even though several other methods exists which fully exploit the information in the hyperspectral  
970 | [reflectance](#)-spectrum, results of the present study still indicates the strength of normalised difference  
971 | indices for extrapolating seasonal dynamics in properties of savanna ecosystems. A number of  
972 | wavelengths [in the reflectance](#)-spectra that are highly correlated to seasonal dynamics in properties of  
973 | semiarid savanna ecosystems have been identified. The relationships between NDSI and ecosystem  
974 | properties were better determined, or at the same level, as results of previous studies exploring  
975 | relationships between hyperspectral [reflectanceHCRFreflectance](#) and ecosystem properties (Kumar,  
976 | 2007; Cho et al., 2007; Mutanga and Skidmore, 2004; Psomas et al., 2011; Ide et al., 2010). By  
977 | studying also the impact from varying viewing and illumination geometry the feasibility and  
978 | applicability of using indices for up-scaling to EO data was evaluated. As such, the results presented  
979 | here offer insights for assessment of ecosystem properties using EO data and this information could be  
980 | used for designing future sensors for observation of ecosystem properties of the Earth.

981 **Acknowledgements**

982 This paper was written within the frame of the project entitled Earth Observation based Vegetation  
983 productivity and Land Degradation Trends in Global Drylands. The project was funded by the Danish  
984 Council for Independent Research (DFF) Sapere Aude programme. The site is maintained by the  
985 Centre de Recherches Zootechniques de Dahra, Institut Sénégalais de Recherches Agricoles (ISRA).

986

987

988 **References**

- 989 Asner, G. P.: Biophysical and Biochemical Sources of Variability in Canopy Reflectance, *Remote*  
990 *Sens. Environ.*, 64, 234-253, [http://dx.doi.org/10.1016/S0034-4257\(98\)00014-5](http://dx.doi.org/10.1016/S0034-4257(98)00014-5), 1998.
- 991 Bicheron, P., and Leroy, M.: Bidirectional reflectance distribution function signatures of major biomes  
992 observed from space, *J. Geophys. Res. -Atmos.*, 105, 26669-26681, 10.1029/2000JD900380, 2000.
- 993 Bowyer, P., and Danson, F. M.: Sensitivity of spectral reflectance to variation in live fuel moisture  
994 content at leaf and canopy level, *Remote Sens. Environ.*, 92, 297-308,  
995 <http://dx.doi.org/10.1016/j.rse.2004.05.020>, 2004.
- 996 Ceccato, P., Gobron, N., Flasse, S., Pinty, B., and Tarantola, S.: Designing a spectral index to estimate  
997 vegetation water content from remote sensing data: Part 1: Theoretical approach, *Remote Sens.*  
998 *Environ.*, 82, 188-197, [http://dx.doi.org/10.1016/S0034-4257\(02\)00037-8](http://dx.doi.org/10.1016/S0034-4257(02)00037-8), 2002.
- 999 Cho, M. A., Skidmore, A., Corsi, F., van Wieren, S. E., and Sobhan, I.: Estimation of green grass/herb  
1000 biomass from airborne hyperspectral imagery using spectral indices and partial least squares regression,  
1001 *Int. J. Appl. Earth Obs. Geoinf.*, 9, 414-424, <http://dx.doi.org/10.1016/j.jag.2007.02.001>, 2007.
- 1002 Cihlar, J., Manak, D., and Voisin, N.: AVHRR bidirectional reflectance effects and compositing,  
1003 *Remote Sens. Environ.*, 48, 77-88, [http://dx.doi.org/10.1016/0034-4257\(94\)90116-3](http://dx.doi.org/10.1016/0034-4257(94)90116-3), 1994.
- 1004 Coburn, C. A., and Peddle, D. R.: A low-cost field and laboratory goniometer system for estimating  
1005 hyperspectral bidirectional reflectance, *Can. J. Remote Sens.*, 32, 244-253, 10.5589/m06-021, 2006.
- 1006 Danson, F. M., Steven, M. D., Malthus, T. J., and Clark, J. A.: High-spectral resolution data for  
1007 determining leaf water content, *Int. J. Remote Sens.*, 13, 461-470, 10.1080/01431169208904049, 1992.
- 1008 Entcheva Campbell, P. K., Middleton, E. M., Corp, L. A., and Kim, M. S.: Contribution of chlorophyll  
1009 fluorescence to the apparent vegetation reflectance, *Sci. Total Environ.*, 404, 433-439,  
1010 <http://dx.doi.org/10.1016/j.scitotenv.2007.11.004>, 2008.
- 1011 Falge, E., Baldocchi, D., Olson, R., Anthoni, P., Aubinet, M., Bernhofer, C., Burba, G., Ceulemans, R.,  
1012 Clement, R., Dolman, H., Granier, A., Gross, P., Grunwald, T., Hollinger, D., Jensen, N. O., Katul, G.,  
1013 Keronen, P., Kowalski, A., Lai, C. T., Law, B. E., Meyers, T., Moncrieff, J., Moors, E., Munger, J. W.,  
1014 Pilegaard, K., Rannik, U., Rebmann, C., Suyker, A., Tenhunen, J., Tu, K., Verma, S., Vesala, T.,  
1015 Wilson, K., and Wofsy, S.: Gap filling strategies for defensible annual sums of net ecosystem  
1016 exchange, *Agric. For. Meteorol.*, 107, 43-69, 2001.
- 1017 Fan, S. M., Wofsy, S. C., Bakwin, P. S., Jacob, D. J., and Fitzjarrald, D. R.: Atmosphere-Biosphere  
1018 Exchange of CO<sub>2</sub> and O<sub>3</sub> in the Central Amazon Forest, *J. Geophys. Res.*, 95, 16851-16864, 1990.
- 1019 Fensholt, R., Sandholt, I., and Rasmussen, M. S.: Evaluation of MODIS LAI, fAPAR and the relation  
1020 between fAPAR and NDVI in a semi-arid environment using in situ measurements, *Remote Sens.*  
1021 *Environ.*, 91, 490-507, <http://dx.doi.org/10.1016/j.rse.2004.04.009>, 2004.
- 1022 Fensholt, R., Sandholt, I., and Stisen, S.: Evaluating MODIS, MERIS, and VEGETATION vegetation  
1023 indices using in situ measurements in a semiarid environment, *IEEE T. Geosci. Remote*, 44, 1774-  
1024 1786, 10.1109/TGRS.2006.875940, 2006.
- 1025 Fensholt, R., Sandholt, I., Proud, S. R., Stisen, S., and Rasmussen, M. O.: Assessment of MODIS sun-  
1026 sensor geometry variations effect on observed NDVI using MSG SEVIRI geostationary data, *Int. J.*  
1027 *Remote Sens.*, 31, 6163-6187, 2010.
- 1028 Feret, J.-B., François, C., Asner, G. P., Gitelson, A. A., Martin, R. E., Bidel, L. P. R., Ustin, S. L., le  
1029 Maire, G., and Jacquemoud, S.: PROSPECT-4 and 5: Advances in the leaf optical properties model  
1030 separating photosynthetic pigments, *Remote Sens. Environ.*, 112, 3030-3043,  
1031 <http://dx.doi.org/10.1016/j.rse.2008.02.012>, 2008.



1032 Foken, T., Gøckede, M., Mauder, M., Mahrt, L., Amiro, B., and Munger, W.: Post-field data quality  
1033 control, in: Handbook of Micrometeorology- A guidebook for Surface Flux Measurement and Analysis,  
1034 edited by: Lee, J. A., Massman, W., and Law, B., Kluwer Academic Publishers, London, 181-203,  
1035 2004.

1036 Gamon, J. A., Peñuelas, J., and Field, C. B.: A narrow-waveband spectral index that tracks diurnal  
1037 changes in photosynthetic efficiency, *Remote Sens. Environ.*, 41, 35-44,  
1038 [http://dx.doi.org/10.1016/0034-4257\(92\)90059-S](http://dx.doi.org/10.1016/0034-4257(92)90059-S), 1992.

1039 Gao, F., Jin, Y., Schaaf, C. B., and Strahler, A. H.: Bidirectional NDVI and atmospherically resistant  
1040 BRDF inversion for vegetation canopy, *IEEE Transactions on Geoscience and Remote Sensing*, 40,  
1041 1269-1278, 10.1109/TGRS.2002.800241, 2002.

1042 Gates, D. M., Keegan, H. J., Schleter, J. C., and Weidner, V. R.: Spectral Properties of Plants, *Appl.*  
1043 *Optics*, 4, 11-20, 1965.

1044 Gitelson, A. A., Merzlyak, M. N., and Lichtenthaler, H. K.: Detection of Red Edge Position and  
1045 Chlorophyll Content by Reflectance Measurements Near 700 nm, *J. Plant Physiol.*, 148, 501-508,  
1046 [http://dx.doi.org/10.1016/S0176-1617\(96\)80285-9](http://dx.doi.org/10.1016/S0176-1617(96)80285-9), 1996.

1047 Gower, S. T., Kucharik, C. J., and Norman, J. M.: Direct and indirect estimation of leaf area index,  
1048 fAPAR, and net primary production of terrestrial ecosystems - a real or imaginary problem?, *Remote*  
1049 *Sens. Environ.*, 70, 29-51, 1999.

1050 Hansen, P. M., and Schjoerring, J. K.: Reflectance measurement of canopy biomass and nitrogen status  
1051 in wheat crops using normalized difference vegetation indices and partial least squares regression,  
1052 *Remote Sens. Environ.*, 86, 542-553, [http://dx.doi.org/10.1016/S0034-4257\(03\)00131-7](http://dx.doi.org/10.1016/S0034-4257(03)00131-7), 2003.

1053 Hapke, B., DiMucci, D., Nelson, R., and Smythe, W.: The cause of the hot spot in vegetation canopies  
1054 and soils: Shadow-hiding versus coherent backscatter, *Remote Sens. Environ.*, 58, 63-68,  
1055 [http://dx.doi.org/10.1016/0034-4257\(95\)00257-X](http://dx.doi.org/10.1016/0034-4257(95)00257-X), 1996.

1056 Hilker, T., Coops, N. C., Nestic, Z., Wulder, M. A., and Black, A. T.: Instrumentation and approach for  
1057 unattended year round tower based measurements of spectral reflectance, *Computers and Electronics in*  
1058 *Agriculture*, 56, 72-84, 10.1016/j.compag.2007.01.003, 2007.

1059 Hilker, T., Coops, N. C., Wulder, M. A., Black, T. A., and Guy, R. D.: The use of remote sensing in  
1060 light use efficiency based models of gross primary production: A review of current status and future  
1061 requirements, *Sci. Total Environ.*, 404, 411-423, <http://dx.doi.org/10.1016/j.scitotenv.2007.11.007>,  
1062 2008.

1063 Hilker, T., Nestic, Z., Coops, N. C., and Lessard, D.: A new automated, multiangular radiometer  
1064 instrument for tower-based observations of canopy reflectance (AMSPEC II), *Instrumentation Science*  
1065 *& Technology*, 38, 319-340, 10.1080/10739149.2010.508357, 2010.

1066 Holben, B., and Fraser, R. S.: Red and near-infrared sensor response to off-nadir viewing, *Int. J.*  
1067 *Remote Sens.*, 5, 145-160, 10.1080/01431168408948795, 1984.

1068 Hsieh, C. I., Katul, G., and Chi, T. W.: An approximate analytical model for footprint estimation of  
1069 scalar fluxes in thermally stratified atmospheric flows, *Adv. Water Res.*, 23, 765-772, 2000.

1070 Huber, S., Koetz, B., Psomas, A., Kneubuehler, M., Schopfer, J. T., Itten, K. I., and Zimmermann, N.  
1071 E.: Impact of multiangular information on empirical models to estimate canopy nitrogen concentration  
1072 in mixed forest, *APPRES*, 4, 043530-043530-043517, 10.1117/1.3435334, 2010.

1073 Huber, S., Tagesson, T., and Fensholt, R.: An automated field spectrometer system for studying VIS,  
1074 NIR and SWIR anisotropy for semi-arid savanna, *Remote Sens. Environ.*, 152, 547-556, 2014.

1075 Huete, A. R., Hua, G., Qi, J., Chehbouni, A., and van Leeuwen, W. J. D.: Normalization of  
1076 multidirectional red and NIR reflectances with the SAVI, *Remote Sens. Environ.*, 41, 143-154,  
1077 [http://dx.doi.org/10.1016/0034-4257\(92\)90074-T](http://dx.doi.org/10.1016/0034-4257(92)90074-T), 1992.

1078 Ide, R., Nakaji, T., and Oguma, H.: Assessment of canopy photosynthetic capacity and estimation of  
1079 GPP by using spectral vegetation indices and the light-response function in a larch forest, *Agric. For.*  
1080 *Meteorol.*, 150, 389-398, 2010.

1081 Inoue, Y., Moran, M. S., and Horie, T.: Analysis of spectral measurements in rice paddies for  
1082 predicting rice growth and yield based on a simple crop simulation model, *Plant Production Science*, 1,  
1083 269–279, 1998.

1084 Inoue, Y., Penuelas, J., Miyata, A., and Mano, M.: Normalized difference spectral indices for  
1085 estimating photosynthetic efficiency and capacity at a canopy scale derived from hyperspectral and  
1086 CO<sub>2</sub> flux measurements in rice, *Remote Sens. Environ.*, 112, 156-172, 2008.

1087 Jacquemoud, S., Verhoef, W., Baret, F., Bacour, C., Zarco-Tejada, P. J., Asner, G. P., François, C., and  
1088 Ustin, S. L.: PROSPECT+SAIL models: A review of use for vegetation characterization, *Remote Sens.*  
1089 *Environ.*, 113, Supplement 1, S56-S66, <http://dx.doi.org/10.1016/j.rse.2008.01.026>, 2009.

1090 Javier García-Haro, F., Camacho-de Coca, F., and Meliá, J.: Retrieving leaf area index from multi-  
1091 angular airborne data, *Annals of Geophysics*, 49, 209-218, 2006.

1092 Jin, H., and Eklundh, L.: A physically based vegetation index for improved monitoring of plant  
1093 phenology, *Remote Sens. Environ.*, 152, 512-525, <http://dx.doi.org/10.1016/j.rse.2014.07.010>, 2014.

1094 Jin, Y., Gao, F., Schaaf, C. B., Xiaowen, L., Strahler, A. H., Bruegge, C. J., and Martonchik, J. V.:  
1095 Improving MODIS surface BRDF/Albedo retrieval with MISR multiangle observations, *IEEE T.*  
1096 *Geosci. Remote*, 40, 1593-1604, 10.1109/TGRS.2002.801145, 2002.

1097 Joiner, J., Guanter, L., Lindstrot, R., Voigt, M., Vasilkov, A. P., Middleton, E. M., Huemmrich, K. F.,  
1098 Yoshida, Y., and Frankenberg, C.: Global monitoring of terrestrial chlorophyll fluorescence from  
1099 moderate-spectral-resolution near-infrared satellite measurements: methodology, simulations, and  
1100 application to GOME-2, *Atmospheric Measuring Techniques*, 6, 2803-2823, doi:10.5194/amt-6-2803-  
1101 2013, 2013.

1102 Kimes, D. S.: Dynamics of Directional Reflectance Factor Distributions for Vegetation Canopies,  
1103 *Appl. Optics*, 22, 1364-1372, 1983.

1104 Kumar, L.: High-spectral resolution data for determining leaf water content in Eucalyptus species: leaf  
1105 level experiments, *Geocarto International*, 22, 3-16, 2007.

1106 Lasslop, G., Reichstein, M., and Papale, D.: Separation of net ecosystem exchange into assimilation  
1107 and respiration using a light response curve approach: critical issues and global evaluation, *Global*  
1108 *Change Biol.*, 16, 187-209, 2010.

1109 Laurent, V. C. E., Verhoef, W., Clevers, J. G. P. W., and Schaepman, M. E.: Inversion of a coupled  
1110 canopy–atmosphere model using multi-angular top-of-atmosphere radiance data: A forest case study,  
1111 *Remote Sens. Environ.*, 115, 2603-2612, <http://dx.doi.org/10.1016/j.rse.2011.05.016>, 2011.

1112 Lee, K., Cohen, WB, Kennedy, RE, Maersperger, TK, Gower, ST Hyperspectral versus multispectral  
1113 data for estimating leaf area index in four different biomes, *Remote Sens. Environ.*, 91, 508-520, 2004.

1114 Leuning, R., Hughes, D., Daniel, P., Coops, N. C., and Newnham, G.: A multi-angle spectrometer for  
1115 automatic measurement of plant canopy reflectance spectra, *Remote Sens. Environ.*, 103, 236-245,  
1116 10.1016/j.rse.2005.06.016, 2006.

1117 LI-COR Biosciences: EDDYPRO Eddy Covariance Software Version 4.0 User's Guide & Reference,  
1118 LI-COR Inc., Lincoln, 200 pp., 2012.

1119 Maignan, F., Bréon, F. M., and Lacaze, R.: Bidirectional reflectance of Earth targets: evaluation of  
1120 analytical models using a large set of spaceborne measurements with emphasis on the Hot Spot,  
1121 *Remote Sens. Environ.*, 90, 210-220, <http://dx.doi.org/10.1016/j.rse.2003.12.006>, 2004.

1122 Martonchik, J. V., Bruegge, C. J., and Strahler, A. H.: A review of reflectance nomenclature used in  
1123 remote sensing, *Remote Sensing Reviews*, 19, 9-20, 10.1080/02757250009532407, 2000.

1124 Mbow, C., Fensholt, R., Rasmussen, K., and Diop, D.: Can vegetation productivity be derived from  
1125 greenness in a semi-arid environment? Evidence from ground-based measurements, *J. Arid Environ.*,  
1126 97, 56-65, <http://dx.doi.org/10.1016/j.jaridenv.2013.05.011>, 2013.

1127 Meroni, M., Rossini, M., Guanter, L., Alonso, L., Rascher, U., Colombo, R., and Moreno, J.: Remote  
1128 sensing of solar-induced chlorophyll fluorescence: Review of methods and applications, *Remote Sens.*  
1129 *Environ.*, 113, 2037-2051, <http://dx.doi.org/10.1016/j.rse.2009.05.003>, 2009.

1130 Milton, E. J., Schaepman, M. E., Anderson, K., Kneubühler, M., and Fox, N.: Progress in field  
1131 spectroscopy, *Remote Sens. Environ.*, 113, Supplement 1, S92-S109,  
1132 <http://dx.doi.org/10.1016/j.rse.2007.08.001>, 2009.

1133 Moncrieff, J. B., Massheder, J. M., de Bruin, H., Elbers, J., Friborg, T., Heusinkveld, B., Kabat, P.,  
1134 Scott, S., Soegaard, H., and Verhoef, A.: A system to measure surface fluxes of momentum, sensible  
1135 heat, water vapour and carbon dioxide, *J. Hydrol.*, 188-189, 589-611, 10.1016/s0022-1694(96)03194-  
1136 0, 1997.

1137 Moncrieff, J. B., R. Clement, J. Finnigan, and Meyers, T.: Averaging, detrending and filtering of eddy  
1138 covariance time series, in: *Handbook of Micrometeorology: A Guide for Surface Flux Measurements*,  
1139 edited by: Lee, X., W. J., Massman and B. E. Law., Kluwer Academic, Dordrecht, 7-31, 2004.

1140 Mutanga, O., and Skidmore, A. K.: Narrow band vegetation indices overcome the saturation problem in  
1141 biomass estimation, *Int. J. Remote Sens.*, 25, 3999-4014, 10.1080/01431160310001654923, 2004.

1142 Myneni, R. B., and Williams, D. L.: On the relationship between FAPAR and NDVI, *Remote Sens.*  
1143 *Environ.*, 49, 200-211, 1994.

1144 Pisek, J., Ryu, Y., Sprintsin, M., He, L., Oliphant, A. J., Korhonen, L., Kuusk, J., Kuusk, A.,  
1145 Bergstrom, R., Verrelst, J., and Alikas, K.: Retrieving vegetation clumping index from Multi-angle  
1146 Imaging SpectroRadiometer (MISR) data at 275 m resolution, *Remote Sens. Environ.*, 138, 126-133,  
1147 <http://dx.doi.org/10.1016/j.rse.2013.07.014>, 2013.

1148 Psomas, A., Kneubühler, M., Huber, S., Itten, K., and Zimmermann, N. E.: Hyperspectral remote  
1149 sensing for estimating aboveground biomass and for exploring species richness patterns of grassland  
1150 habitats, *Int. J. Remote Sens.*, 32, 9007-9031, 10.1080/01431161.2010.532172, 2011.

1151 Qi, J., Chehbouni, A., Huete, A. R., Kerr, Y. H., and Sorooshian, S.: A modified soil adjusted  
1152 vegetation index, *Remote Sens. Environ.*, 48, 119-126, 1994.

1153 Rasmussen, M. O., Göttsche, F. M., Diop, D., Mbow, C., Olesen, F. S., Fensholt, R., and Sandholt, I.:  
1154 Tree survey and allometric models for tiger bush in northern Senegal and comparison with tree  
1155 parameters derived from high resolution satellite data, *Int. J. Appl. Earth Obs. Geoinf.*, 13, 517-527,  
1156 10.1016/j.jag.2011.01.007, 2011.

1157 Richter, K., Atzberger, C., Hank, T. B., and Mauser, W.: Derivation of biophysical variables from  
1158 Earth observation data: validation and statistical measures, *APPRES*, 6, 063557-063551-063557-  
1159 063523, 10.1117/1.JRS.6.063557, 2012.

1160 Roberto, C., Lorenzo, B., Michele, M., Micol, R., and Cinzini, P.: Optical Remote Sensing of  
1161 Vegetation Water Content, in: *Hyperspectral Remote Sensing of Vegetation*, edited by: Thenkabail, P.  
1162 S., Lyon, J. G., and Huete, A., CRC Press, Taylor and Francis Group, Boca Raton, FL, 227-244, 2012.

1163 Rouse, J. W., Haas, R. H., Schell, J. A., Deering, D. W., and Harlan, J. C.: Monitoring the Vernal  
1164 Advancement of Retrogradation of Natural Vegetation, Type III, Final Report, Greenbelt, MD, 1974.

1165 Sandmeier, S., Müller, C., Hosgood, B., and Andreoli, G.: Physical Mechanisms in Hyperspectral  
1166 BRDF Data of Grass and Watercress, *Remote Sens. Environ.*, 66, 222-233,  
1167 [http://dx.doi.org/10.1016/S0034-4257\(98\)00060-1](http://dx.doi.org/10.1016/S0034-4257(98)00060-1), 1998.

1168 Schaepman-Strub, G., Schaepman, M. E., Painter, T. H., Dangel, S., and Martonchik, J. V.: Reflectance  
1169 quantities in optical remote sensing—definitions and case studies, *Remote Sens. Environ.*, 103, 27-42,  
1170 <http://dx.doi.org/10.1016/j.rse.2006.03.002>, 2006.

1171 Schopfer, J., Dangel, S., Kneubühler, M., and Itten, K.: The Improved Dual-view Field Goniometer  
1172 System FIGOS, *Sensors*, 8, 5120-5140, 2008.

1173 Sims, D. A., and Gamon, J. A.: Estimation of vegetation water content and photosynthetic tissue area  
1174 from spectral reflectance: a comparison of indices based on liquid water and chlorophyll absorption  
1175 features, *Remote Sens. Environ.*, 84, 526-537, 2003.

1176 Sjöström, M., Ardö, J., Eklundh, L., El-Tahir, B. A., El-Khidir, H. A. M., Hellström, M., Pilesjö, P.,  
1177 and Seaquist, J.: Evaluation of satellite based indices for gross primary production estimates in a sparse  
1178 savanna in the Sudan, *Biogeosciences*, 6, 129-138, 2009.

1179 Soudani, K., Hmimina, G., Dufrière, E., Berveiller, D., Delpierre, N., Ourcival, J.-M., Rambal, S., and  
1180 Joffre, R.: Relationships between photochemical reflectance index and light-use efficiency in  
1181 deciduous and evergreen broadleaf forests, *Remote Sens. Environ.*, 144, 73-84, 2014.

1182 Tagesson, T., Eklundh, L., and Lindroth, A.: Applicability of leaf area index products for boreal  
1183 regions of Sweden, *Int. J. Remote Sens.*, 30, 5619-5632, 2009.

1184 Tagesson, T., Mastepanov, M., Tamstorf, M. P., Eklundh, L., Schubert, P., Ekberg, A., Sigsgaard, C.,  
1185 Christensen, T. R., and Ström, L.: High-resolution satellite data reveal an increase in peak growing  
1186 season gross primary production in a high-Arctic wet tundra ecosystem 1992-2008, *Int. J. Appl. Earth  
1187 Obs. Geoinf.*, 18, 407-416, 2012.

1188 Tagesson, T., Fensholt, R., Copley, F., Guiro, I., Horion, S., Ehammer, A., and Ardö, J.: Dynamics in  
1189 carbon exchange fluxes for a grazed semi-arid savanna ecosystem in West Africa, *Agr. Ecosyst.  
1190 Environ.*, 205, 15-24, <http://dx.doi.org/10.1016/j.agee.2015.02.017>, 2015a.

1191 Tagesson, T., Fensholt, R., Guiro, I., Rasmussen, M. O., Huber, S., Mbow, C., Garcia, M., Horion, S.,  
1192 Sandholt, I., Rasmussen, B. H., Götsche, F. M., Ridler, M.-E., Olén, N., Olsen, J. L., Ehammer, A.,  
1193 Madsen, M., Olesen, F. S., and Ardö, J.: Ecosystem properties of semi-arid savanna grassland in West  
1194 Africa and its relationship to environmental variability, *Global Change Biol.*, 21, 250-264, doi:  
1195 10.1111/gcb.12734, 2015b.

1196 Thenkabail, P. S., Smith, R. B., and De Pauw, E.: Hyperspectral Vegetation Indices and Their  
1197 Relationships with Agricultural Crop Characteristics, *Remote Sens. Environ.*, 71, 158-182,  
1198 [http://dx.doi.org/10.1016/S0034-4257\(99\)00067-X](http://dx.doi.org/10.1016/S0034-4257(99)00067-X), 2000.

1199 Thenkabail, P. S., Enclona, E. A., Ashton, M. S., and Van Der Meer, B.: Accuracy assessments of  
1200 hyperspectral waveband performance for vegetation analysis applications, *Remote Sens. Environ.*, 91,  
1201 354-376, 2004.

1202 Thenkabail, P. S., Lyon, J. G., and Huete, A.: Advances in hyperspectral remote sensing of vegetation  
1203 and agricultural croplands, in: *Hyperspectral Remote Sensing of Vegetation*, edited by: Thenkabail, P.  
1204 S., Lyon, J. G., and Huete, A., CRC Press, Taylor and Francis Group, Boca Raton, FL, 3-35, 2012.

1205 Tucker, C. J.: Red and photographic infrared linear combinations for monitoring vegetation, *Remote  
1206 Sens. Environ.*, 8, 127-150, [http://dx.doi.org/10.1016/0034-4257\(79\)90013-0](http://dx.doi.org/10.1016/0034-4257(79)90013-0), 1979.

1207 van Leeuwen, W. J. D., Huete, A. R., and Laing, T. W.: MODIS Vegetation Index Compositing  
1208 Approach: A Prototype with AVHRR Data, *Remote Sens. Environ.*, 69, 264-280,  
1209 [http://dx.doi.org/10.1016/S0034-4257\(99\)00022-X](http://dx.doi.org/10.1016/S0034-4257(99)00022-X), 1999.  
1210 Verhoef, W., and Bach, H.: Coupled soil-leaf-canopy and atmosphere radiative transfer modeling to  
1211 simulate hyperspectral multi-angular surface reflectance and TOA radiance data, *Remote Sens.*  
1212 *Environ.*, 109, 166-182, <http://dx.doi.org/10.1016/j.rse.2006.12.013>, 2007.  
1213 Vickers, D., and Mahrt, L.: Quality control and flux sampling problems for tower and aircraft data, *J.*  
1214 *Atmos. Ocean. Tech.*, 14, 152-526, 1997.  
1215 Webb, E. K., Pearman, G. I., and Leuning, R.: Correction of the flux measurements for density effects  
1216 due to heat and water vapour transfer, *Q. J. Roy. Meteor. Soc.*, 106, 85-100, 1980.  
1217 Wilczak, J. M., Oncley, S. P., and Stage, S. A.: Sonic anemometer tilt correction algorithms, *Bound.-*  
1218 *Lay. Meteorol.*, 99, 127-150, 2001.  
1219

1220

1221 **Tables**

1222 Table 1. Information regarding about the sensor set-up of for the measured environmental variables. HCRF is hemispherical conical  
 1223 reflectance factor; GPP is gross primary productivity; LUE is light use efficiency; and FAPAR is fraction of photosynthetically active  
 1224 radiation absorbed by the vegetation. Min and Max are minimum and maximum values measured, respectively; DW is dry weight; C  
 1225 is carbon; and MJ is megajoule.

<u>Variable</u>	<u>Unit</u>	<u>Sensors</u>	<u>Sensor company</u>	<u>Data size</u>	<u>Aggregation method</u>	<u>Data gaps</u>	<u>Min</u>	<u>Max</u>
<u>Hyperspectral reflectanceHCRF</u>	<u>-</u>	<u>Fieldspec 3</u>	<u>ASD Inc., Colorado, USA</u>	<u>371</u>	<u>Daily median</u>	<u>31%</u>	<u>0</u>	<u>1</u>
<u>Herbaceous biomass</u>	<u>g DW m<sup>-2</sup></u>	<u>-</u>	<u>-</u>	<u>12</u>	<u>Daily mean 28 plots</u>	<u>-</u>	<u>0</u>	<u>223</u>
<u>GPP</u>	<u>g C d<sup>-1</sup></u>	<u>LI-7500, GILL R3</u>	<u>LI-COR Inc., Lincoln, USA; Gill instruments, Hampshire, UK</u>	<u>285</u>	<u>Daily sums</u>	<u>56%</u>	<u>-14.22</u>	<u>-0.22</u>
<u>LUE</u>	<u>g C MJ<sup>-1</sup></u>	<u>LI-7500, GILL R3</u>	<u>LI-COR Inc., Lincoln, USA; Gill instruments, Hampshire, UK</u>	<u>272</u>	<u>Daily estimates</u>	<u>28%</u>	<u>0.02</u>	<u>1.89</u>
<u>FAPAR</u>	<u>-</u>	<u>Quantum SKP 215</u>	<u>Skye instruments Ltd., Llandridod wells, UK</u>	<u>369</u>	<u>Daily averages 10:00-16:00</u>	<u>1%</u>	<u>0.07</u>	<u>0.77</u>

1226  
1227

1228 | Table 42. Wavelengths of the hemispherical conical reflectance factors (reflectances-HCRF) ( $\rho_i, j$ ) used  
 1229 | in the normalized difference spectral indices (NDSI) that generated the strongest correlations with  
 1230 | ecosystem properties. DW is dry weight; FAPAR is the fraction of photosynthetically active radiation  
 1231 | absorbed by the vegetation; AVG is average; SD is standard deviation; RMSE is root-mean-square-  
 1232 | error.

Ecosystem property	Sample size	$\rho_i$	$\rho_j$	$R^2$	<u>Observation</u> <u>(AVG<math>\pm</math>SD)</u>	RMSE
Biomass ( <u>g DW m<sup>-2</sup></u> )	12	587	705	0.88 $\pm$ 0.07	<u>153<math>\pm</math>59</u>	28.4 $\pm$ 8.7
Gross primary productivity ( <u>g C m<sup>-2</sup> d<sup>-1</sup></u> )	285	518	556	0.86 $\pm$ 0.02	<u>-4.3<math>\pm</math>4.0</u>	1.5 $\pm$ 0.1
Light use efficiency ( <u>g C MJ<sup>-1</sup></u> )	272	688	436	0.81 $\pm$ 0.02	<u>0.53<math>\pm</math>0.65</u>	0.26 $\pm$ 0.02
FAPAR	369	399	1295	0.81 $\pm$ 0.02	<u>0.41<math>\pm</math>0.16</u>	0.06 $\pm$ 0.003

1233  
1234

## Figures

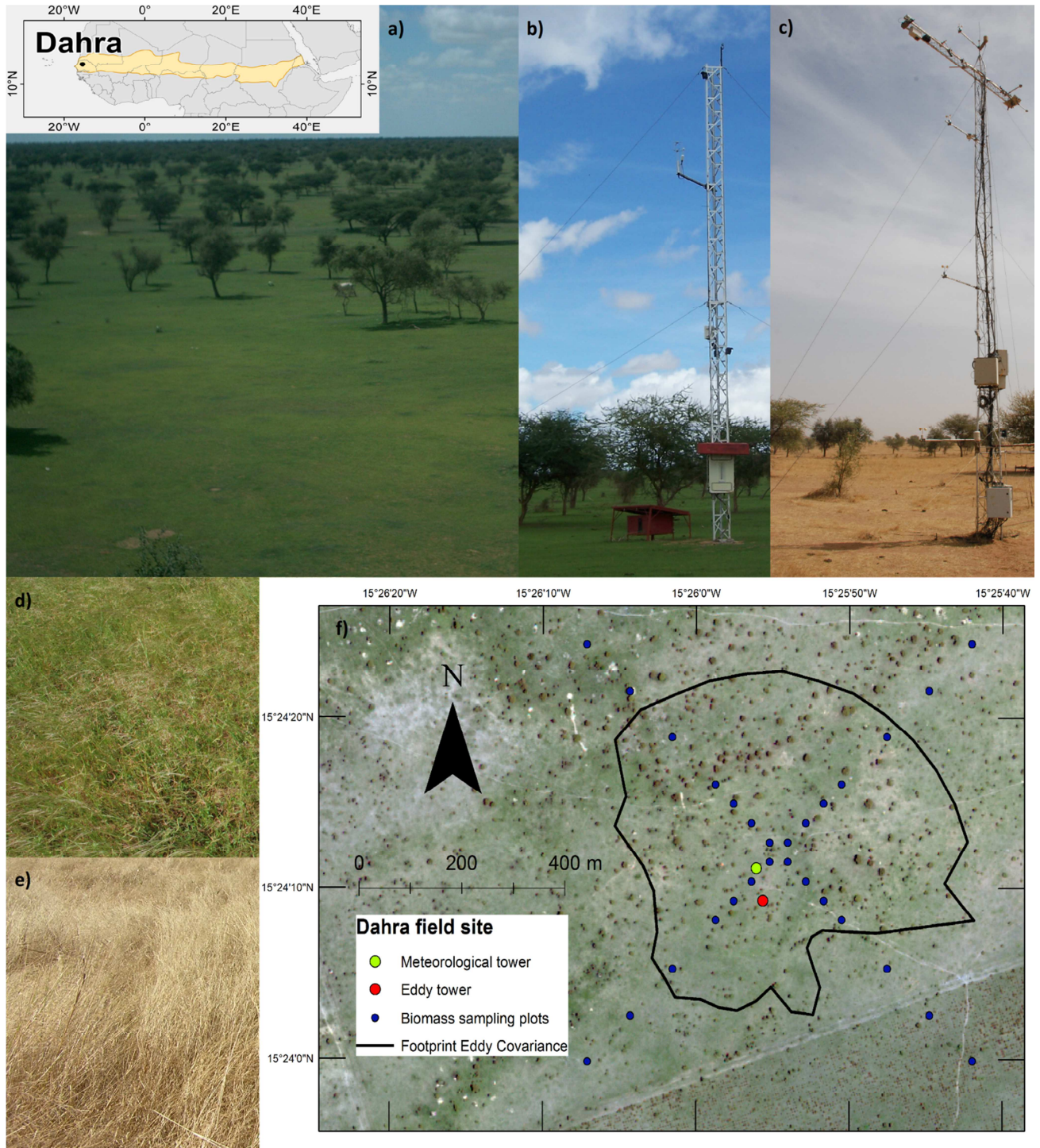
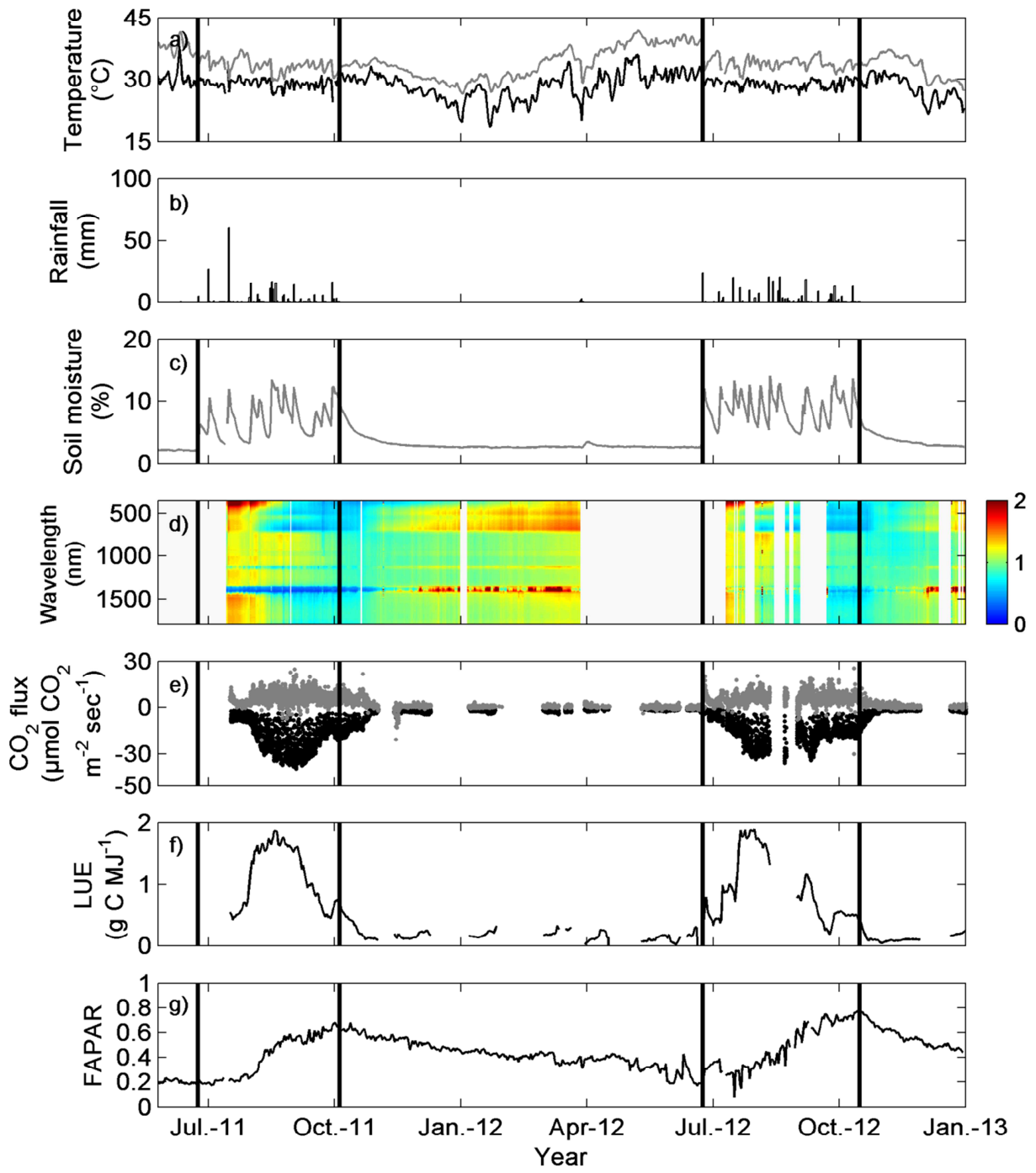


Figure 1. Map and photos of the Dahra field site and the measured areas, and maps over the Dahra field site and tower set up for the eddy covariance tower (left), and the meteorological

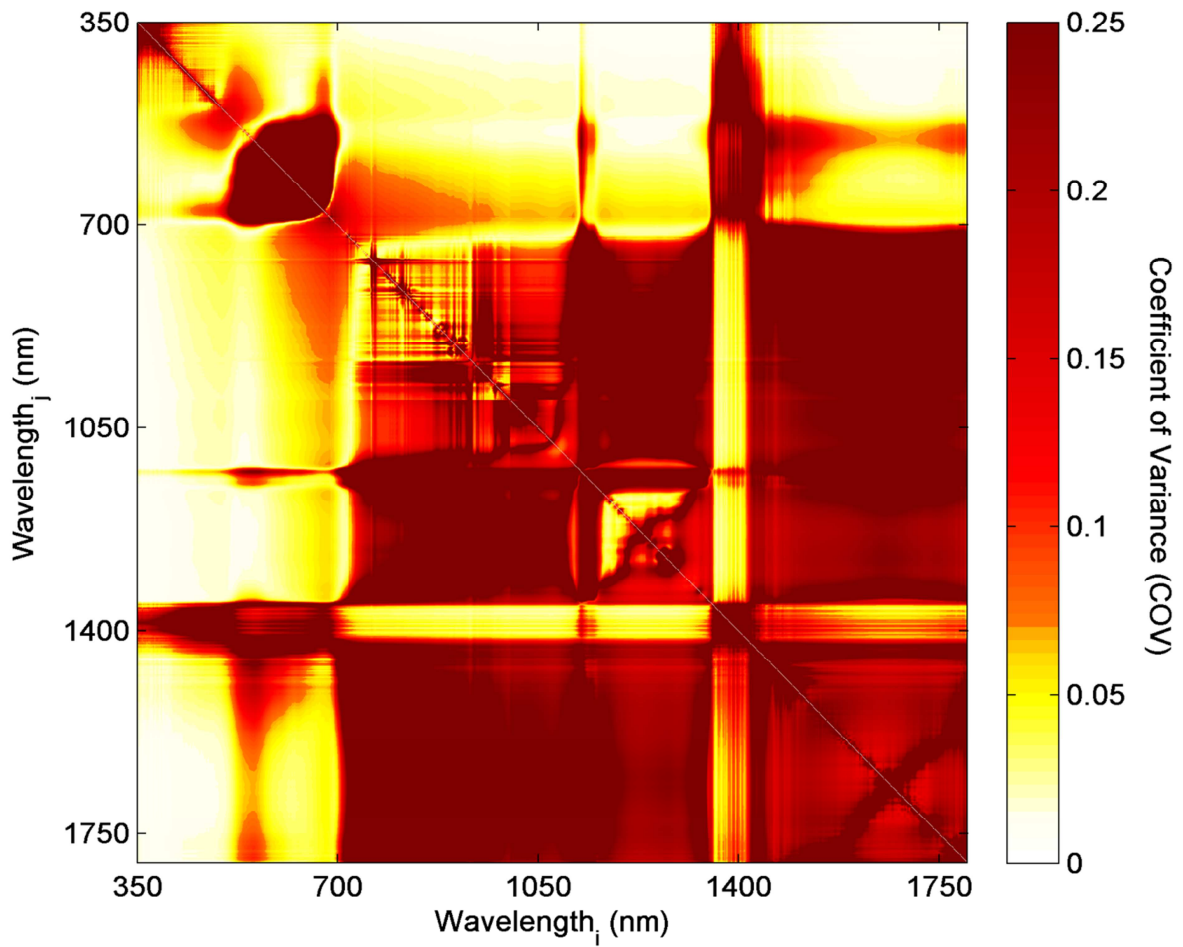


1239 ~~tower with the spectroradiometers (right). The map shows the location of Dahra within the Sahel~~  
1240 ~~(orange area). -a) Picturephoto of the footprint of the eddy covariance (EC) tower; b) picturephoto of the~~  
1241 ~~EC tower; c) picturephoto of the meteorological tower with the spectroradiometers; d) picturephoto of~~  
1242 ~~the instantaneous field of view (fetchIFOV) of the spectroradiometers during the rainy season; e)~~  
1243 ~~picturephoto of the fetchIFOV of the spectroradiometer during the beginning of the dry season; and f)~~  
1244 ~~Quickbird image from the Dahra field site from 11 September 2011 showing the location of the~~  
1245 ~~meteorological tower, the EC tower, the biomass sampling plots and the footprint of the EC~~  
1246 ~~measurements. The EC footprint area is the median 70% cumulative flux distance from the eddy~~  
1247 ~~covariance tower. The overview picturephotos of the EC tower and its footprint and the picture of the~~  
1248 ~~eddy covariance tower showisare taken during the rainy season whereas the picture-photo of the~~  
1249 ~~meteorological tower shows the late dry season. ~~The map shows the location of Dahra within the Sahel~~~~  
1250 ~~(orange area).~~  
1251

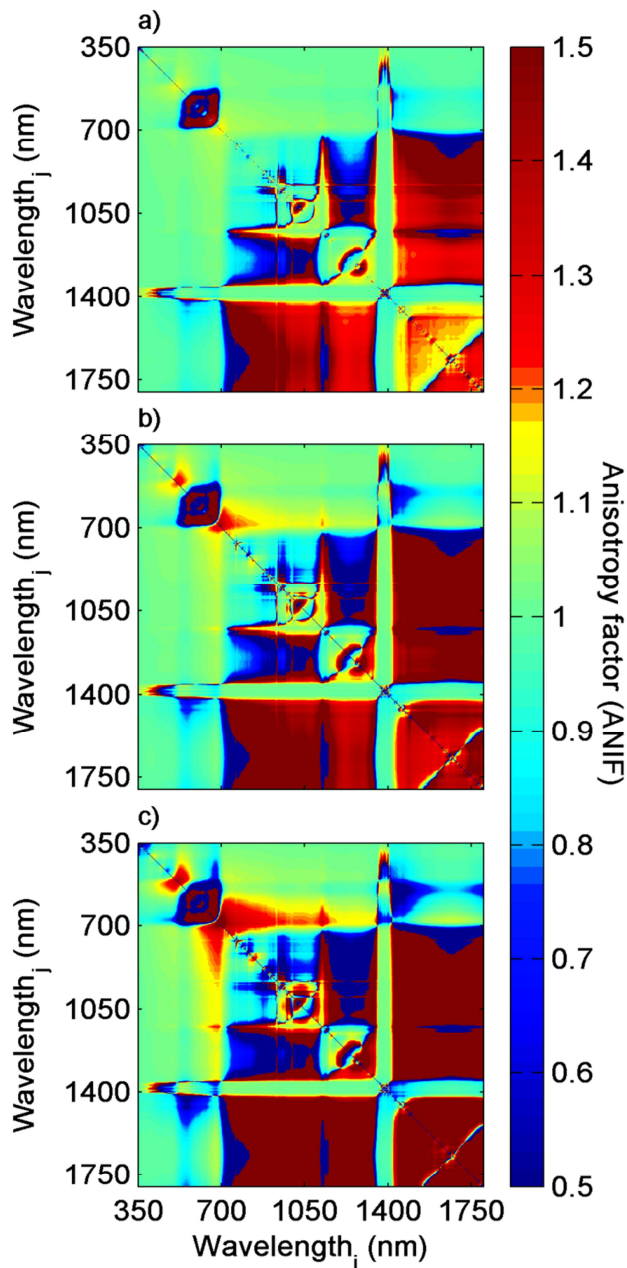


1252  
 1253 Figure 2. Time series of the measured variables: a) daily averaged air temperature (black line), and soil  
 1254 temperature at 0.05 m depth (grey line), b) daily sums of rainfall, c) daily average of soil moisture at  
 1255 0.05 m depth, d) hyperspectral hemispherical conical reflectance factor (reflectanceHCRF) normalized

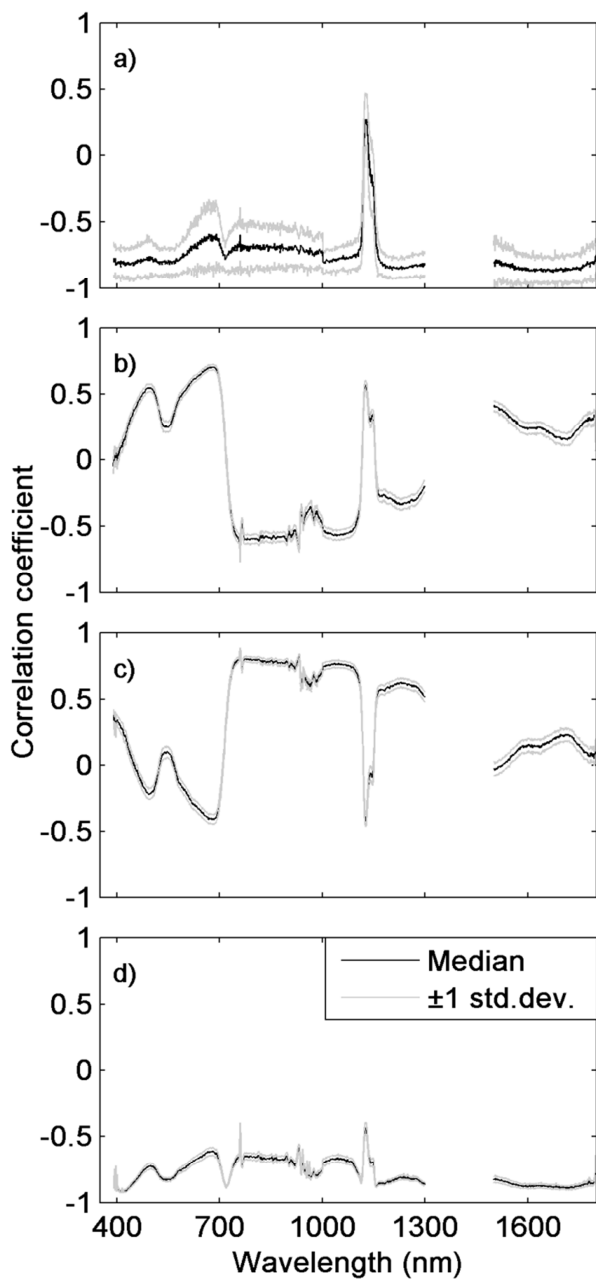
1256 | by calculating the ratio between daily median [reflectanceHCRF](#) for each wavelength (350-1800 nm)  
1257 | and the average [reflectanceHCRF](#) for the entire measurement period, e) gross primary productivity  
1258 | (GPP) (black dots) and ecosystem respiration (grey dots), f) the light use efficiency (LUE), and g) the  
1259 | fraction of photosynthetically active radiation absorbed by the vegetation (FAPAR). The black vertical  
1260 | lines are the start and end of the rainy seasons (first and final day of rainfall). The gaps are caused by  
1261 | technical issues due to loss of power supply, broken sensors or filtering of data due to bad weather  
1262 | conditions.  
1263



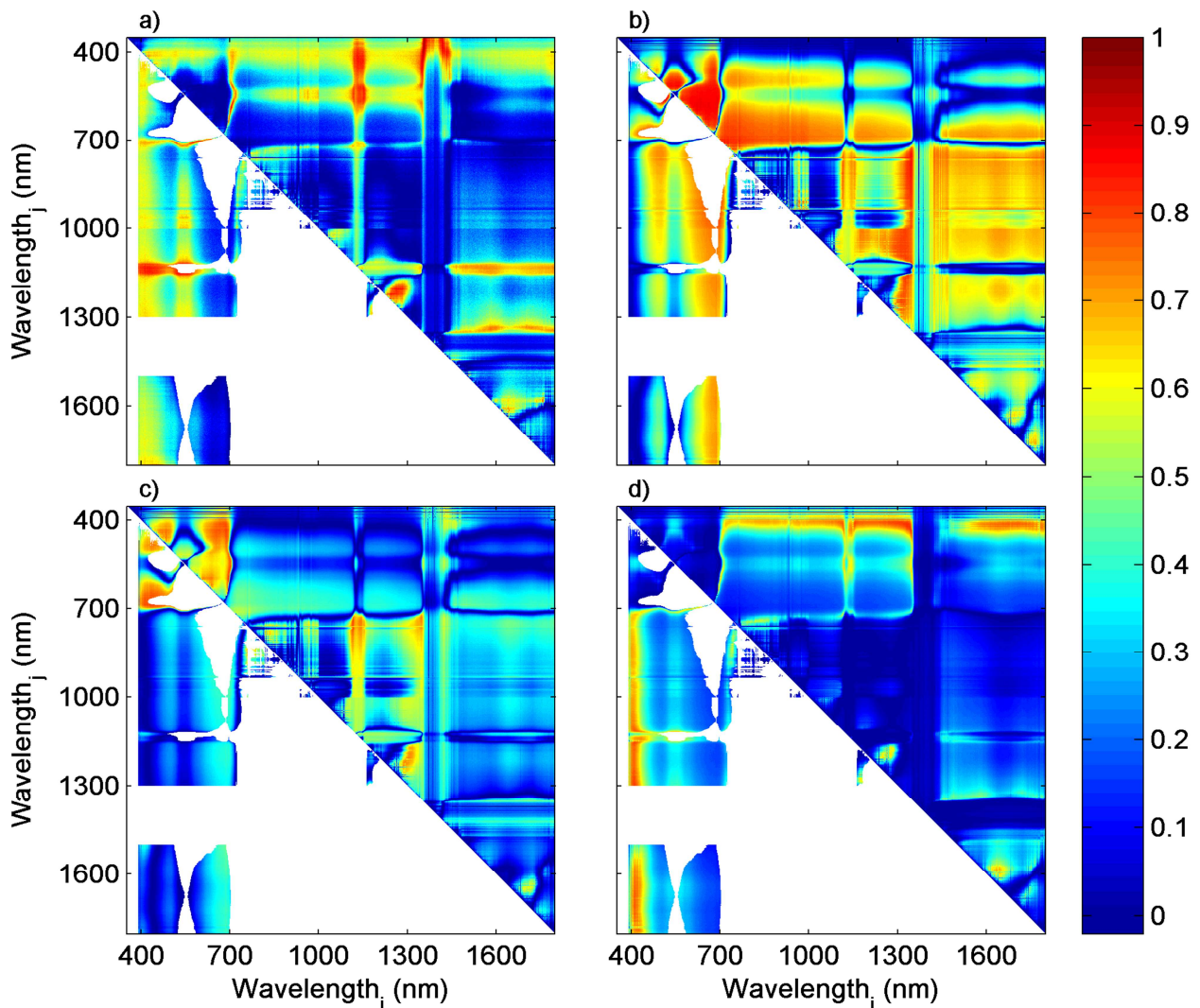
1264  
 1265 Figure 3. The coefficient of variation (COV), i.e. the ratio between daily standard deviation and the  
 1266 daily mean (measurements taken between 8:00 and 18:00), for different normalised difference spectral  
 1267 index (NDSI) wavelength ( $i, j$ ) combinations for 12 days at the peak of the growing season 2011 (day of  
 1268 year 237-251;  $n=576$ ). The COV indicates how strongly the NDSI are affected by variable sun angles.  
 1269



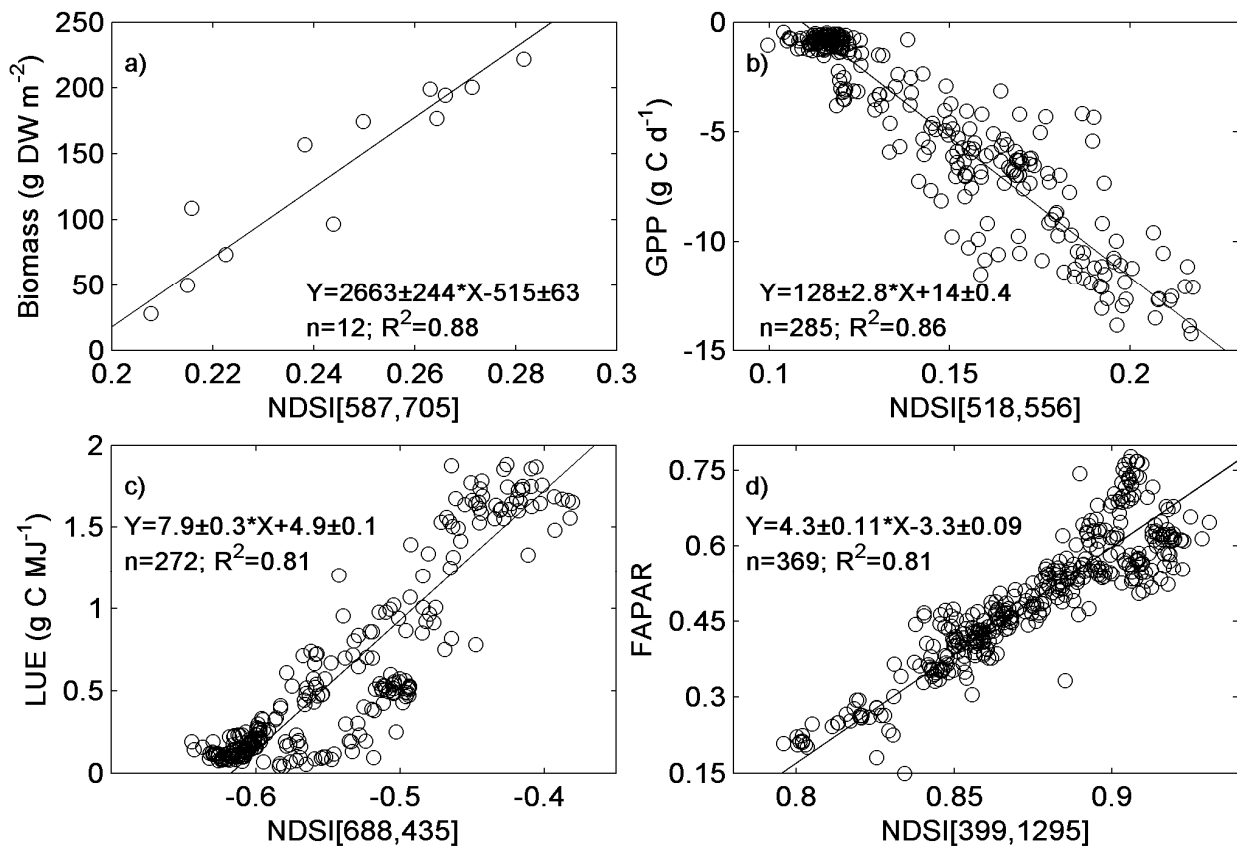
1270  
 1271 | Figure 4. The anisotropy factor (ANIF) for different normalised difference spectral index (NDSI)  
 1272 | wavelength ( $i, j$ ) combinations for 15 days at the peak of the growing season 2011 (day of year 237-251)  
 1273 | for the different sensor viewing angles: a) 15°, b) 30°, and c) 45°. The sensor is pointing east and west  
 1274 | in the lower left and upper right corners of each plot, respectively. In order not to include effects of  
 1275 | solar zenith angles in the analysis, only data measured between 12:00 and 14:00 were used in the ANIF  
 1276 | calculations (n=48).  
 1277  
 1278



1279  
 1280 Figure 5. Median correlation coefficient ( $\pm 1$  standard deviation) between seasonal dynamics in  
 1281 hyperspectral [hemispherical conical reflectance factors](#) ([reflectanceHCRF](#)) 2011-2012 and a) dry  
 1282 weight biomass ( $n=12$ ;  $\text{g m}^{-2}$ ), b) gross primary productivity (GPP) ( $n=285$ ;  $\text{g C day}^{-1}$ ), c) light use  
 1283 efficiency (LUE) ( $n=272$ ;  $\text{g C MJ}^{-1}$ ), and d) fraction of photosynthetically active radiation absorbed by  
 1284 the vegetation (FAPAR) ( $n=369$ ).  
 1285  
 1286



1287  
 1288 | Figure 6. Coefficient of determination ( $R^2$ ) between **normalised difference spectral index (-NDSI)** and  
 1289 a) dry weight biomass (n=12; g m<sup>-2</sup>), b) gross primary productivity (GPP) (n=285; g C day<sup>-1</sup>), c) light  
 1290 use efficiency (LUE) (n=272; g C MJ<sup>-1</sup>), and d) fraction of photosynthetically active radiation  
 1291 absorbed by the vegetation (FAPAR) (n=369). The upper right half of each image shows the unfiltered  
 1292  $R^2$  values, whereas the lower left half shows filtered  $R^2$ , based on the filtering criteria described under  
 1293 Subsect. 2.6.  
 1294



1295  
 1296 | Figure 7. The least square linear regressions with the strongest relationships between the normalised  
 1297 | difference spectral index (NDSI) and a) dry weight biomass, b) gross primary productivity (GPP), c)  
 1298 | light use efficiency (LUE), and d) fraction of photosynthetically active radiation absorbed by the  
 1299 | vegetation (FAPAR). In the equations, the slope and intercepts ( $\pm 1$  standard deviation) is given.